Wall turbulence manipulation by large-scale streamwise vortices

By GAETANO IUSO[1], MICHELE ONORATO[1],
PIER GIORGIO SPAZZINI[2]
AND GAETANO MARIA DI CICCA[1]

[1]DIASP, Politecnico di Torino, C.so Duca degli Abruzzi, 24, I 10129 Torino, Italy

[2]CNR, CSDF c/o DIASP, Politecnico di Torino, C.so Duca degli Abruzzi, 24,
I 10129 Torino, Italy

This paper describes an experimental study of the manipulation of a fully developed turbulent channel flow through large-scale streamwise vortices originated by vortex generator jets distributed along the wall in the spanwise direction. Apart from the interest in flow management itself, an important aim of the research is to observe the response of the flow to external perturbations as a technique for investigating the structure of turbulence. Considerable mean and fluctuating skin friction reductions, locally as high as 30% and 50% respectively, were measured for an optimal forcing flow intensity. Mean and fluctuating velocity profiles are also greatly modified by the manipulating large-scale vortices; in particular, attenuation of the turbulence intensity was measured. Moreover the flow manipulation caused an increase in longitudinal coherence of the wall organized motions, accompanied by a reduced frequency of burst events, demonstrated by a reduction of the velocity time derivative PDFs and by an higher intermittency. A strong transversal periodic organization of the flow field was observed, including some typical behaviours in each of the periodic boxes originated by the interaction of the vortex pairs. Results are interpreted and discussed in terms of management of the near-wall turbulent structures and with reference to the wall turbulence regeneration mechanisms suggested in the literature.

1. Introduction

Although recurring organized motions in turbulent boundary layers, such as low-speed streaks and vortical structures (e.g. quasi-longitudinal, hairpin, arch vortices), have been observed and studied for many years, their dynamics and initiation mechanisms are still the object of debate. Whereas it has long been recognized that vortices cause the velocity streaks by advecting the mean velocity gradient (see e.g. Blackwelder & Eckelmann 1979) and that several vortices are associated with each streak (see e.g. Jimenez & Moin 1991), the physical processes leading to the creation of new vortical structures is still not understood to a satisfactory degree. This understanding is crucial for developing strategies for turbulent boundary layers in order to control skin friction, wall heat flux and aeroacoustic properties. A detailed and still up-to-date review about turbulence regeneration mechanisms in near-wall flows can be found in the book edited by Panton (1997). Essentially, the proposed regeneration mechanisms for self-maintaining turbulence may be grouped in two possible regeneration cycles: the wall cycle requiring the active presence of a parent vortex near the wall (Bernard

& Wallace 1997; Smith & Walker 1997; Zhou *et al.* 1997; Hanratty & Papavassiliou 1997; Adrian, Meinhart & Tomkins 2000); and the vortex-free streak cycle based on the instability of the low-speed streaks (Kim, Kline & Reynolds 1971; Hamilton, Kim & Waleffe 1995; Waleffe & Kim 1997; Jimenez & Pinelli 1999; Schoppa & Hussain 1997, 2000). For the latter cycle the wall contribution is limited to the generation of the mean velocity shear layer.

With increasing knowledge of the mechanisms of turbulence regeneration in wall-bounded flows, turbulence control strategies are becoming the subject of investigation in many laboratories. The most straightforward approaches are to simply prevent vortex regeneration or to counteract the active dynamics of already existing structures. The latter implies small-scale feedback control schemes relying on suitable actuators triggered by local sensors. Vortex regeneration may instead be controlled by stabilizing or weakening the basic flow streaks (Jimenez & Pinelli 1999). This approach is attractive because of the possibility of large-scale control, wherein numerous streaks may be simultaneously stabilized by a single larger-scale forcing (Schoppa & Hussain 2000).

Some papers relevant to the results discussed in the present work are listed in the following subsections, in which 'non-canonical' large-scale wall boundary conditions are imposed on the flow, including wall suction and/or blowing (§ 1.1), wall cross-flows (§ 1.2) and vortical flows (§ 1.3), after which the present experiment is described (§ 1.4).

1.1. *Wall suction and blowing*

Antonia *et al.* (1988) experimentally examined the effect of wall suction on the organized motions of a turbulent boundary layer. They observed by flow visualization a significant reduction in the spanwise oscillation of the low-speed streaks while their streamwise persistence increased. The finding that even very small rates of suction lead to a stabilization of the streaks was supported by the reduced number of ejections observed in the flow. This increase in streak coherence was associated with the reduction (measured in a parallel experiment) of Reynolds stresses, temperature variances and heat fluxes induced by suction.

Control of turbulent boundary layers through uniform blowing and suction was performed by Sumitani & Kasagi (1995) and Park & Choi (1999). Results from these studies indicate that uniform blowing from the wall can decrease the skin friction and increase the turbulence intensities, while a uniform suction has almost exactly opposite effects.

Yoshida *et al.* (1999) performed a DNS in order to study the response of coherent structures to local injection or suction below a low-speed streak. They found that while injection increases the turbulence energy, suction attenuates both the low- and the high-speed streaks, leading thus to turbulence suppression.

1.2. *Cross-flow*

Jung, Mangiavacchi & Akhavan (1992) conducted a DNS study ($Re_c = 3000$) of a turbulent channel flow subject either to an oscillatory spanwise cross-flow or to spanwise oscillatory motion of one of the channel walls. Their results indicate a 40% reduction in skin friction drag when the non-dimensional period of oscillation T^+ was set to 100. The oscillations also gave rise to a 40% reduction in the streamwise component of the Reynolds stress, with no significant increases in the spanwise component. The root mean squares of the fluctuating velocity components also experienced significant reductions: u' (14%), v' (30%) and w' (35%). The results

were independent of whether the oscillations were generated by a cross-flow or by the motion of the channel wall. Jung *et al.* (1992) observed that this turbulence reduction occurred because of the decrease in the number and intensity of turbulent bursts in the oscillatory channel compared to the unperturbed flow. These results were experimentally confirmed by Laadhari, Skandaji & Morel (1994) for a boundary layer flow at $Re_\theta = 950$. The latter authors explain that the continuous shifting of the longitudinal vortices to different positions relative to the wall velocity streaks weakens the intensity of the streaks injecting high-speed fluid into low-speed streaks and low-speed fluid into high-speed regions.

The effect of the wall oscillation amplitude on the total energy balance was investigated by Baron & Quadrio (1996) using DNS of a turbulent channel flow. For an oscillation period of $T^+ = 100$ they found 10% net energy saving with wall oscillation amplitudes of $Q_x/4h$, where Q_x is the flow rate and h is the turbulent channel half-height.

An experimental investigation of changes in the turbulent boundary layer structure with a spanwise wall oscillation was carried out by Choi, DeBisschop & Clayton (1998) (see also Choi 2000). Their results indicate that the inner-scaled mean velocity profiles collapse into a single curve in the viscous sublayer region, but they are shifted upwards in the logarithmic region as the wall oscillation frequency is increased. The inner-scaled velocity profiles show, moreover, that the linear region of the viscous sublayer increases up to $y^+ = 10$ for the maximum oscillation frequency (7 Hz) of the experiment. In agreement with previously mentioned DNS and laboratory experiments a reduction of 45% in the skin friction coefficient was measured with wall oscillations. Moreover, infrared images show that several low-speed streaks coalesce into a single streak as the wall oscillates, increasing the streak spacing by about 45%, whereas the duration of the streaks T^+ is multiplied by a factor 4 (when the wall oscillates near the optimum conditions). It was also shown in Choi *et al.*'s (1998) and Choi's (2000) experiments that the meandering motion of the streaks was greatly reduced while the wall was oscillating. The authors related this mechanism of drag reduction to the spanwise vorticity generated by the periodic Stokes layer over the oscillating wall. This net generated spanwise vorticity affects by induction the mean boundary layer profile by reducing the mean velocity gradient (and thus the mean skin friction) within the viscous sublayer, $y^+ < 15$, and by increasing the velocity outside, $y^+ > 15$, hence shifting the logarithmic velocity profile upwards. At the same time, the realignment of longitudinal vortices over the oscillating wall reduces the streamwise component of the vorticity in the near-wall region, weakening the near-wall ejection and sweep activity. More recently, we (see Di Cicca *et al.* 2002*b*) performed a PIV experiment on a turbulent boundary layer over a spanwise oscillating flat plate. The frequency and the amplitude of the wall oscillations were 100 wall time units and 320 wall lengths respectively. In that paper the observed reductions in near-wall turbulence activity could be related to a weakening of the low-speed streak, an increase of their spacing and a reduction of VISA events.

Kresov & Plesniak (1999) also examined the modifications of the near-wall structures in a laboratory three-dimensional turbulent boundary layer. A spanwise shear on a two-dimensional boundary layer was generated through the spanwise translation of a flat plate in which a transversal belt mechanism was included. The result was that the spanwise shear reduced the main streak length by as much as 50% with increasing spanwise shear, while streak spacing remained relatively constant. Streamwise mean velocity profiles showed an increasing velocity deficit as the cross-flow was increased; profiles of turbulent quantities in the inner region of the boundary layer indicated

increases of u'^2, v'^2, $-\overline{uv}$ with increasing spanwise shear out to $y/\delta < 0.4$. However, an initial decrease in u'^2 was observed in the near-wall region at weak cross-flow levels.

1.3. *Vortical flow*

Soldati, Fulgosi & Banerjee (1999) used numerical simulations to analyse the influence of large-scale electro-hydrodynamical streamwise vortical flows superimposed on a plane Poiseuille flow. Their vortical flow had a spanwise periodicity of 340 wall units. Analysis of the results thus obtained indicated that the application of the electrostatic control provided a transient drag reduction of about 6–7%; no significant change of the near-wall flow streaky structure was observed. Soldati *et al.* (1999) concluded that further analysis was required in order to investigate the interaction between the control flow and the structures in turbulent boundary layers.

Schoppa & Hussain (1998), using DNS of a turbulent channel flow, obtained skin friction reduction through large-scale forcing. They found 20% friction drag reduction for imposed counter-rotating streamwise vortices and 50% reduction for colliding spanwise wall jets. The forcing flow had a transversal wavelength of 400 wall units; the largest effect was obtained at a perturbation amplitude of only 6% of the channel centreline velocity. Schoppa & Hussain (1998) attributed the drag reduction to the forcing-induced suppression of an underlying streak instability mechanism which is considered to be the vorticity source leading to the regeneration of the near-wall quasi-longitudinal vortices.

1.4. *Present experiment*

The experiment described in the present paper was performed within the framework of the research programme at the Department of Aerospace Engineering of Politecnico di Torino on the subject of flow control (see e.g. Iuso & Onorato 1995; Di Cicca *et al.* 1999; Onorato *et al.* 2000). The idea driving the experiment is that, in order to contribute to the clarification of the leading mechanisms of wall turbulence and to examine the viability of turbulence control for technological applications in the future, it is important to investigate the response of wall turbulence structures to external physical perturbations. In particular, in the present experiment the basic flow is a fully developed turbulent channel flow and the forcing flow consists of pairs of counter-rotating large-scale streamwise vortices with their axis in the vicinity of the channel horizontal centreplane. The vortices are produced by a suitable array of vortex generator jets (VGJs) located on one of the channel walls. The resulting flow displays – in the spanwise direction – different behaviours which can be related to wall flows in the presence of weak blowing, weak cross-flow and weak suction. The VGJ technique has already been successfully used in flow separation control problems (see e.g. Johnston & Nishi 1990).

This flow perturbation technique was suggested by the numerical experiment of Schoppa & Hussain (1998). As already mentioned in §1.3, in a similar situation they predicted by DNS a large friction drag reduction. To the authors' knowledge (see also Gad-el-Hak 2000), this finding has not yet been confirmed by a physical experiment.

2. Experimental setup

2.1. *The experimental facility*

The measurements were performed in a bidimensional Plexiglas air channel located in the 'Modesto Panetti' Aerodynamics Laboratory of Politecnico di Torino. This
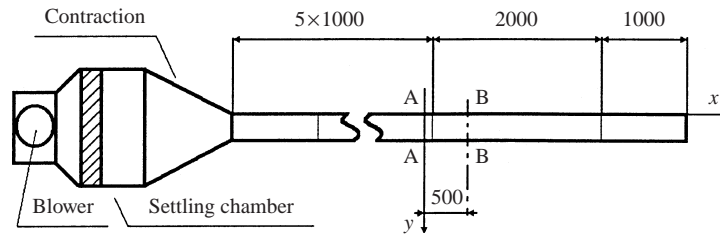
FIGURE 1. Sketch of the experimental facility. A–A: jet injection section, see figure 2.
B–B: main measurement section. All dimensions in mm.

channel has a cross-section of $2 \times 28\,\mathrm{cm}^2$, thus an aspect ratio of 14 which guarantees the bidimensionality of the mean flow, and a length of 8 m. Data were collected in various sections, all of which are located between 5 and 6 m from the channel inlet, i.e. over 250 hydraulic diameters downstream of the inlet section and over 100 hydraulic diameters upstream of the exit. This range of positions guarantees that the channel flow is fully developed and rules out possible exit effects. The channel is made of seven separate elements; the sixth, containing the test section, covers the distance between 5 and 7 m from the channel inlet; its upper wall is wider than the channel, which allows it to be moved in the spanwise direction. The measurement instruments were mounted at fixed positions with respect to this wall, so it was possible to perform measurements along the whole channel cross-section in order to explore the spanwise structure of the flow. The flow could also be explored in the wall-normal direction by using a suitable probe positioner driven by a stepper motor. A centrifugal blower was positioned upstream of the channel and fed a square settling chamber, connected to the channel entry through a two-dimensional convergent characterized by a contraction ratio of 16 : 1. In order to avoid transmission of vibrations from the blower to the channel, a rubber ribbon was inserted between the blower exit and the settling chamber entry. The whole apparatus was insulated from the laboratory floor by rubber blocks in order to prevent the transmission of vibrations from the blower to the test section through the floor. In figure 1 a sketch of the experimental apparatus is given.

The jets for generating the pairs of counter-rotating streamwise vortices were injected via ten 2 mm diameter holes drilled through the channel upper wall; the holes were spaced 30 mm apart from each other and lie in a plane normal to the wall and to the basic flow direction. The holes were alternately inclined by angles of $\pm 45°$; the jet injection section was positioned 4.95 m downstream of the channel entrance, i.e. 5 cm upstream of the test section element. A compressed air reservoir feeds the pneumatic line, characterized by a regulator valve and a floating element flow meter which allow respectively the jet mass flow rate to be changed and measured. A distribution box placed after the flow meter exit splits the total jet mass flow into 10 parts and feeds the five jet couples by means of 10 rubber tubes. Figure 2 is a sketch of the jet injection channel cross-section as seen by an observer looking from the channel outlet into the channel itself. In figures 1 and 2 the reference system is also defined; the origin of the x-axis is at the jet injection section, the origin of the z-axis is at the channel centreline and the y-axis originates from the channel upper wall and points downwards. The interaction between the cross-flow jets and the channel main flow is expected to generate, downstream of the injection section, an array of pairs of counter-rotating vortices as sketched in figure 2.
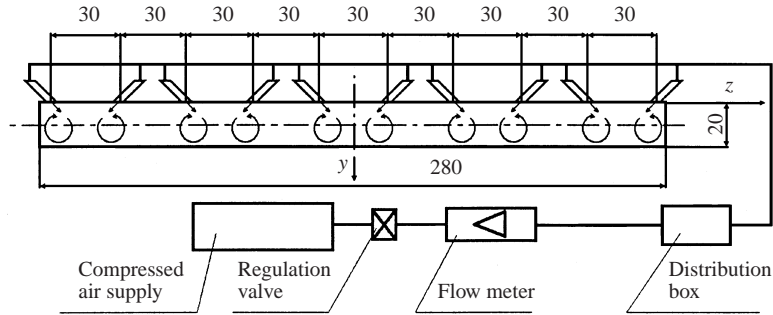
FIGURE 2. Sketch of the vortex generation system. Jet injection section A–A. All dimensions in mm.

2.2. *The measurement techniques*

Time-resolved skin friction data were collected by a hot-wire shear stress probe flush-mounted to the wall. The sensor lies on a cylindrical Plexiglas substrate and its central part is positioned over a cylindrical cavity with diameter and depth both equal to 1 mm. The presence of the cavity reduces heat losses to the substrate and hence increases the probe's precision and frequency response. The sensor is made of 5 μm tungsten-coated platinum wire and is approximately 1.2 mm long, which corresponds to 22 wall units ($\Delta z^+ = 22$) at the Reynolds number of the present experiment. Alfredsson *et al.* (1988) recommend a maximum sensor length Δz^+ of 10–20 units, while Shah & Antonia (1987) found no changes in skin friction fluctuation measurements when varying Δz^+ from 3 to 45. The probe is powered and driven by a Dantec 55M01 high-precision CTA bridge; the overheat ratio employed was equal to 1.8. All data were collected by a National Instruments PCI-MIO-16-XE-10 16-bit DAQ board and stored for subsequent processing on PC files. Skin friction time histories consisted of 2^{20} data points each and were sampled at 12 kHz.

Calibration of the probe was performed in the channel itself under basic flow conditions (VGJs off), at the same position as the measurements. Under such conditions the test section flow is a fully developed channel flow for which it is possible to compute the mean skin friction by simply measuring the static pressure gradient along the channel. Calibration data are approximated by a fourth-order polynomial; figure 3 shows a typical calibration curve for the wall stress probe. Several calibrations were performed on the same probe; comparison of their results shows a slight oscillation band of the calibration curves, which gives an estimate of about 5% for the skin friction measurement uncertainty. A similar probe was tested in a non-canonical flow by Spazzini *et al.* (1999), showing a satisfactory agreement with results from oil fringe interferometric method. The angular response of the probe is also of relevance for the present work, as a single sensor probe is to be used in a flow where weak three-dimensional effects are present, as will be shown. In order to check this angular response, the probe was rotated with respect to the channel axis over the range $\pm 180°$; figure 4 shows the ratio of the skin friction measured by the probe to the actual skin friction as a function of the misalignment angle β at a Reynolds number (with respect to the channel centreline velocity and the channel half-height, $Re = (U_C H/2)/\nu$ of 3600. It can be observed that the curve is well approximated by a cosine function, which implies that the sensor has a low sensitivity to flow misalignments in the $\pm 15°$ range, where the maximum misalignment error is within 7%. It will be shown (see §3.2.1) that three-dimensional effects due to the flow control imply angles β lower than 8°.
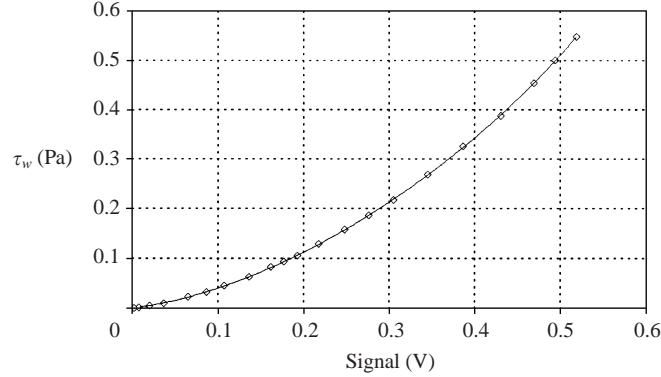
FIGURE 3. Typical skin friction probe calibration curve.
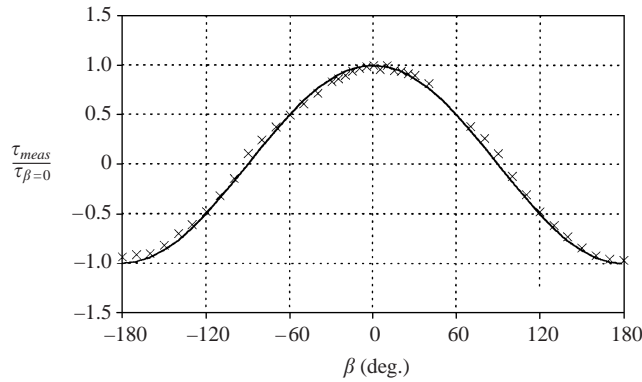
FIGURE 4. Response of the skin friction probe to skewed mean flow.
Solid line: cosine law; crosses: experimental data.

A double flattened Preston tube was used to measure the mean wall shear stress direction. Figure 5(*a*) shows a schematic of the tube, which has a lateral dimension of 2.5 mm and a thickness of 0.4 mm. Pressures from the two sides of the tube were measured by a SETRA model 239 capacitive pressure transducer with ± 125 Pa full range and a nominal 0.14% FS accuracy. This probe was calibrated *in situ* by rotating it by known angles β within the basic flow. Figure 5(*b*) shows its directional calibration curve. The calibration variable is defined as

$$F_{r,l} = \frac{(p_r - p_l)}{(\frac{1}{2}(p_r + p_l) - p_x)}$$

where p_r, p_l are the pressures measured on the right and left sides of the probe, respectively, and p_x is a reference wall static pressure.

The skin friction probes were mounted only on the movable (upper) wall; measurements on the lower wall were simulated by placing the jet injectors on the opposite wall.

Velocity profiles were measured by a standard Dantec 55P11 single hot-wire probe driven by a Dantec 55M01 high-precision CTA bridge; the overheat ratio was equal to 1.8; data were collected by the same acquisition board as used for the skin friction measurements. The spanwise length of the sensor was 1.2 mm, corresponding to $\Delta z^+ = 22$, only slightly higher than the upper limit ($\Delta z^+ = 20$) recommended by
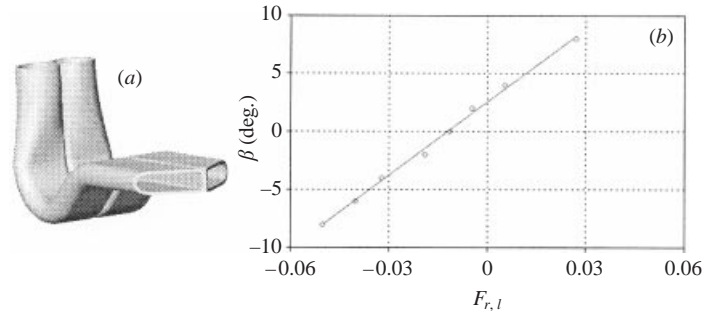
FIGURE 5. (*a*) Sketch of the probe for mean skin friction direction measurement; (*b*) typical directional calibration curve.

Blackwelder & Haritodinis (1983) in order to avoid spatial-averaging effects. In this case, 2^{19} data points were acquired at a sampling frequency of 14 kHz. The mean flow direction in horizontal planes (x, z) at different wall distances was also separately measured using a miniature directional probe, built by soldering two tubes having external diameter of 0.6 mm, with an apex angle equal to 90°. The sensitivity of the probe was high enough to measure with good accuracy flow direction to within 0.5°. The same pressure transducer and calibration procedure used for the double Preston tube were used for this probe. Note that this probe was used only in regions where the wall-normal mean velocity component was negligible with respect to the spanwise component.

In order to obtain information about the mean structural organization of the manipulated flow in the test section, a rake for total pressure measurements was built with eight tubes (external diameter 0.6 mm, internal diameter 0.3 mm) spaced 2.5 mm from each other. The rake spanned the vertical dimension of the channel and could be tranversed in the spanwise direction by moving the upper wall. The eight pressure signals were sent through a Scanivalve to the capacitive pressure transducer described above. The rake tubes were disposed so that their axes were parallel to the channel axis. Although three-dimensional effects were found to be weak, implying small deviation angles, the total pressure maps obtained from this probe have been, in general, considered only from a qualitative standpoint, in order to obtain a visualization of the flow field. Only the results referring to the basic flow, for which the flow direction is known, have been considered as quantitatively reliable.

In order to provide information about the effect of the perturbing vortical flow on the near-wall turbulence lateral scale and on the strength of the low-speed streaks, some DPIV results obtained from a parallel experiment in a boundary layer flow are presented in Appendix C.

2.3. *Experimental conditions*

The experiments described in the following were performed at a Reynolds number of 3600, based on the channel half-height, $H/2$, and the centreline velocity, U_C, which corresponds to a Reynolds number based on the friction velocity of the basic flow and on the channel half-height, Re_τ, of 180. The spanwise distance (30 mm) between the jets corresponds, for this Reynolds number and for the case of the basic flow, to 550 wall units. The total jet mass flow rate was typically 3% of the channel mass flow rate; due to the small diameter of the holes (2 mm), the jet exit velocity was of the order of 5 times the channel centreline velocity ($U_C = 5.4 \, \text{m s}^{-1}$).
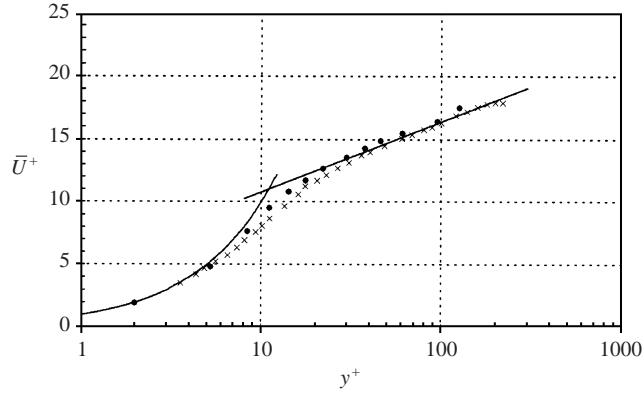
FIGURE 6. Basic flow: mean velocity profile. Solid line: law of the wall. Crosses: results from the present experiment. Circles: results from Wei & Willmarth (1989).

Measurements for both the basic and manipulated flows were collected at several stations downstream of the jet injection section.

3. Results

In §3.1 the important properties of the basic flow are presented, while §3.2 deals with the manipulated flow. Analysis and discussion of the results is given in §4.

3.1. *The basic flow*

Figures 6 and 7 show statistical results relating to the basic flow. Figure 6 displays the streamwise mean velocity ($\overline{U}$) profile; data are scaled with inner variables. The profile exhibits the expected logarithmic behaviour for $y^+ = 30$ to the channel centre. The overall profile agrees satisfactorily with LDV data reported in the literature (Wei & Willmarth 1989). Good agreement may also be observed in figure 7 concerning the root mean square of the streamwise velocity fluctuation, u'. Figure 8 shows the measured spanwise distribution of the mean skin friction coefficient ($\overline{C_f}$) and of the standard deviation of its fluctuating component (c'_f). As can be seen, uniform distributions of $\overline{C_f}$ and c'_f characterize the cross-section for a distance of about ± 100 mm from the longitudinal axis of the channel. Secondary flow effects are evident from the reduction of $\overline{C_f}$ close to the channel lateral vertical walls.

The ratio between the root mean square of the skin friction fluctuation and the skin friction mean value ($c'_f/\overline{C_f}$) has been measured at 0.31, in agreement with literature results: careful measurements by Alfredsson *et al.* (1988) provided values ranging from 0.36 to 0.40.

3.2. *The manipulated flow*

Moving now to the manipulated flow, figure 9 displays results obtained by scanning the channel sections at $x/H = 7.7, 25, 43, 53$ with the total pressure rake. In figure 9 constant-C_{p_t} contour lines in the range $-60 \leqslant z \leqslant 60$ mm are reported, where $C_{p_t} = (p_{t_i} - p_{ref})/q_C$; p_{t_i} is the pressure measured by the rake at the generic point i, p_{ref} is a constant reference static pressure and q_C is the dynamical pressure at the channel centreline for the unmanipulated flow. Figure 9(*a*) is a plot of the basic flow iso-C_{p_t} lines, while figures 9(*b*)–9(*e*) refer to the manipulated flow in the various sections downstream of the jets. The results in figure 9 were obtained with a total jet
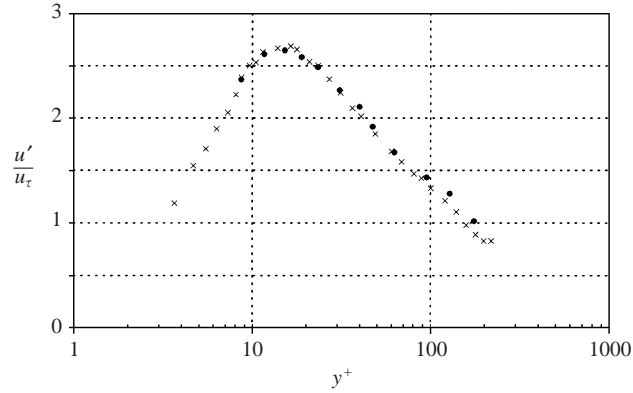
FIGURE 7. Basic flow: turbulence profiles. Crosses: results from the present experiment. Circles: results from Wei & Willmarth (1989).
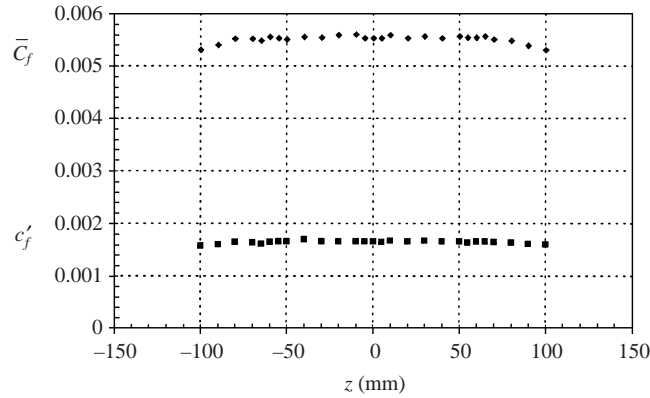
FIGURE 8. Basic flow: spanwise distribution of skin friction coefficient mean value (diamonds) and fluctuating component (squares).

mass flow rate Q_j as small as 3% of the channel mass flow rate before the injection Q_c, $Q_j/Q_c = 0.031$.

The first point to note is that, while in the basic case the flow structure is symmetric with respect to the channel centreplane ($y = 10$ mm) and essentially uniform in the z-direction, the manipulated case exhibits a much more complex structure. Indeed, the symmetry with respect to the horizontal centreplane is lost, mainly due to the fact that injection is from a single side, whilst a strong organization of the flow, repeated in the spanwise direction, appears. In order to better understand the flow organization visualized in figure 9, it can be useful to look in parallel at the results presented in figure 10, also referring to the manipulated flow with $Q_j = 0.031Q_c$, at $x/H = 25$; the figure reports the skin friction direction β along the span of the channel upper and lower walls. β is the angle between the skin friction direction and the x-axis; it is defined to be positive when it generates positive values of the transversal component of skin friction, according to the reference axis. The visualizations presented in figure 9 and the data in figure 10 suggest the following reasonable scenario for the flow structure in the measurement cross-planes. The closed iso-C_{p_t} lines in the channel central region provide evidence of counter-rotating vortical structures originated by the interaction between the jets and the main flow. The two vortices generate, between
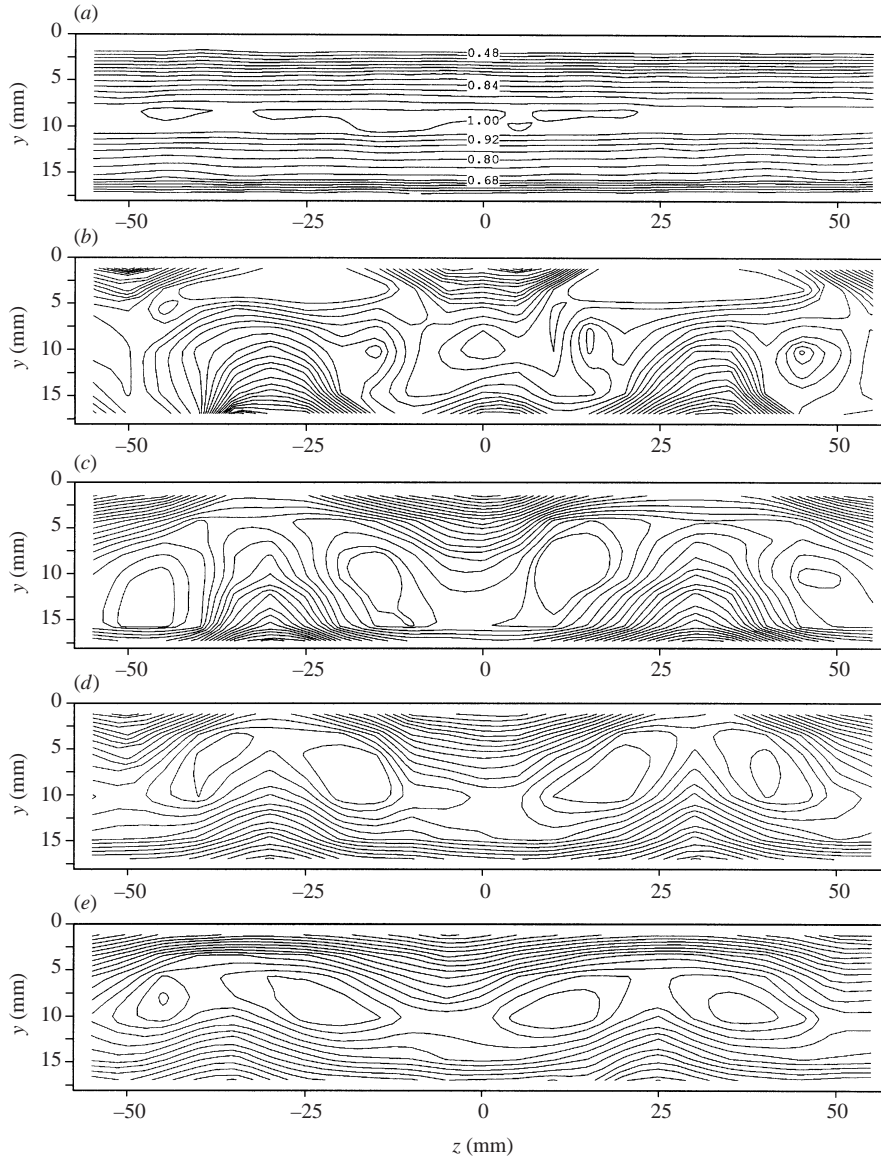
FIGURE 9. Iso-C_{p_t} lines in the measurement section: (*a*) unmanipulated flow; (*b–e*) manipulated flow, respectively at $x/H = 7.7, 25, 43, 53$. $Q_j/Q_c = 0.031$.

them, a flow moving away from the upper wall, while in the external region a flow directed towards the wall is present. Beneath their axis, the vortices generate cross-flows, which are more intense on the upper wall (see figure 10), where the jets are operated. This flow structure is then repeated along the channel span. The zero crossings of the β distribution and the sign of the skin friction direction (figure 10) are globally consistent with the flow structure shown in figure 9(*c*) and furthermore reveals, as can be expected, the existence of secondary vortical structures with their axes at about $z = \pm 8$ mm, visible on the upper wall only. The secondary vortices are not evident in figures 9(*c*), 9(*d*) and 9(*e*) because of their small scale with respect to the pressure rake spatial resolution. In the first measurement section (figure 9*b*)
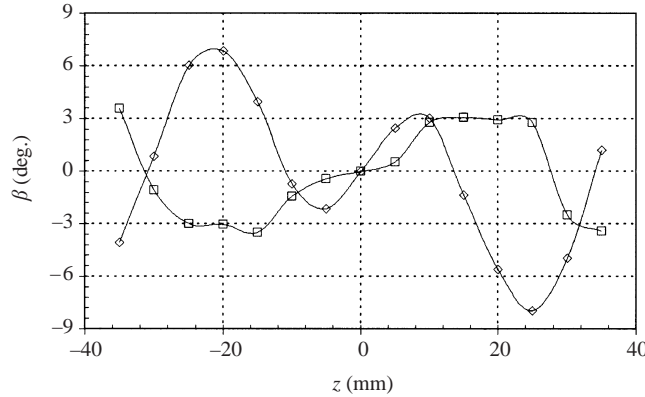
FIGURE 10. Spanwise skin friction direction distribution on the channel walls. Manipulated flow, $Q_j/Q_c = 0.031$, $x/H = 25$. Diamonds: upper wall results; squares: lower wall results.

the vortical flow structures do not yet appear to be fully organized: most of the observed disturbance is due to a first interaction of the jets with the main flow. Going downstream, the generated vortices preserve their coherence and the distance between the central pair of counter-rotating vortices appears to increase slightly. At $x = 53H$ the vortical flow is still observable, though the flow exhibits a general tendency to relax to undisturbed conditions. Most of the analysis performed in the following refers to the case of $Q_j/Q_c = 0.031$ and to the section visualized in figure 9(*c*), far enough from the jets, where the vortices are well formed.

Figures 9 and 10 also allow the spanwise scale of the perturbing flow to be estimated. It turns out that this scale, for $Re_c = 3600$, is of the order of 500–600 wall units, i.e. much larger than the typical turbulent structure scales in the near-wall region: a value of 100 viscous units is the standard spacing between low-speed streaks in the buffer layer.

The very small values (less than 8°) of β in figure 10 indicate furthermore that the wall shear stress component in the spanwise direction can be expected to have very small values. A similar analysis was performed for the bulk velocity direction using the miniature direction probe; a maximum flow direction deviation from the channel axis direction of approximately 7° was also found.

The small values of β, moreover, guarantee the validity of the skin friction and velocity measurements that will be presented in the following sections, which were performed using single sensor probes.

3.2.1. *Skin friction measurements*

Figures 11(*a*), 11(*b*) and 11(*c*) display the measured percent variation, with respect to the unperturbed flow, in mean skin friction coefficient $\overline{C_f}$ and in the root mean square value of its fluctuation component c'_f, as a function of the jet mass flow rate Q_j/Q_c. Results refer to the upper wall of the channel section $25H$ downstream of the jets, for different spanwise positions, namely at $z = 0$ (up-flow region, figure 11*a*), $z = 15$ mm (cross-flow region, figure 11*b*) and $z = 30$ mm (down-flow region, figure 11*c*). In figure 11(*a*) it is possible to observe that, for $z = 0$, the behaviour of $\overline{C_f}$ and c'_f is essentially the same: for both drag and turbulence the reductions start to be evident from $Q_j/Q_c \approx 0.008$ and persist up to $Q_j/Q_c \approx 0.04$; higher $\overline{C_f}$ and c'_f than the unperturbed case are present for $Q_j/Q_c > 0.04$. The peak reduction ($\approx 18\%$ for $\overline{C_f}$
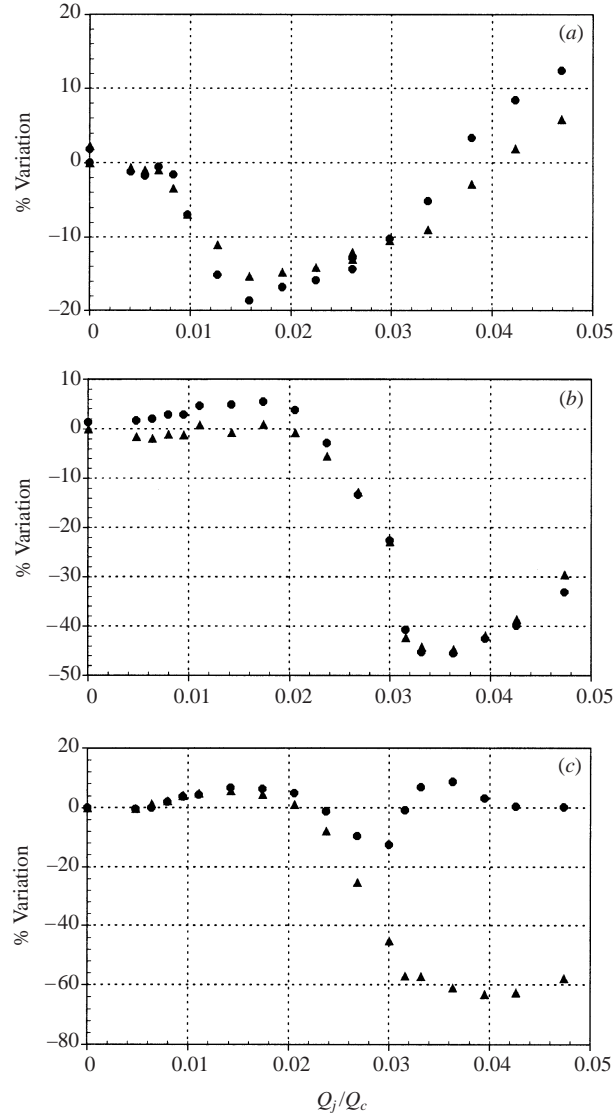
FIGURE 11. $\overline{C_f}$ (circles) and c'_f (triangles) variations as a function of mass flow rate at $x = 25H$ on the upper wall. (*a*) $z = 0$; (*b*) $z = 15\,\text{mm}$; (*c*) $z = 0\,\text{mm}$. $Re = 3600$.

and $\approx 15\%$ for c'_f) is reached at $Q_j/Q_c \approx 0.016$. At $z = 15\,\text{mm}$, figure 11(*b*) displays a similar situation, although higher mass flow ratios are needed in order to produce reductions ($Q_j/Q_c > 0.02$). At this position, on the other hand, the maximum reductions are of about 45% for both $\overline{C_f}$ and c'_f and are observed at $Q_j/Q_c \approx 0.033$–0.036. Finally at $z = 30\,\text{mm}$, figure 11(*c*), the situation appears to be quite different as a very high reduction (more than 60%) is obtained in c'_f at $Q_j/Q_c \approx 0.04$ while $\overline{C_f}$ experiences a much lower reduction (about 15%) for a different mass flow rate, namely $Q_j/Q_c \approx 0.031$. Moreover, $\overline{C_f}$ exhibits an oscillating behaviour, with increasing $\overline{C_f}$ for $Q_j/Q_c > 0.032$.

Qualitatively similar results have been obtained on the wall opposite to the jets (lower wall, with reference to figure 9*c*), where more modest mean and fluctuating skin
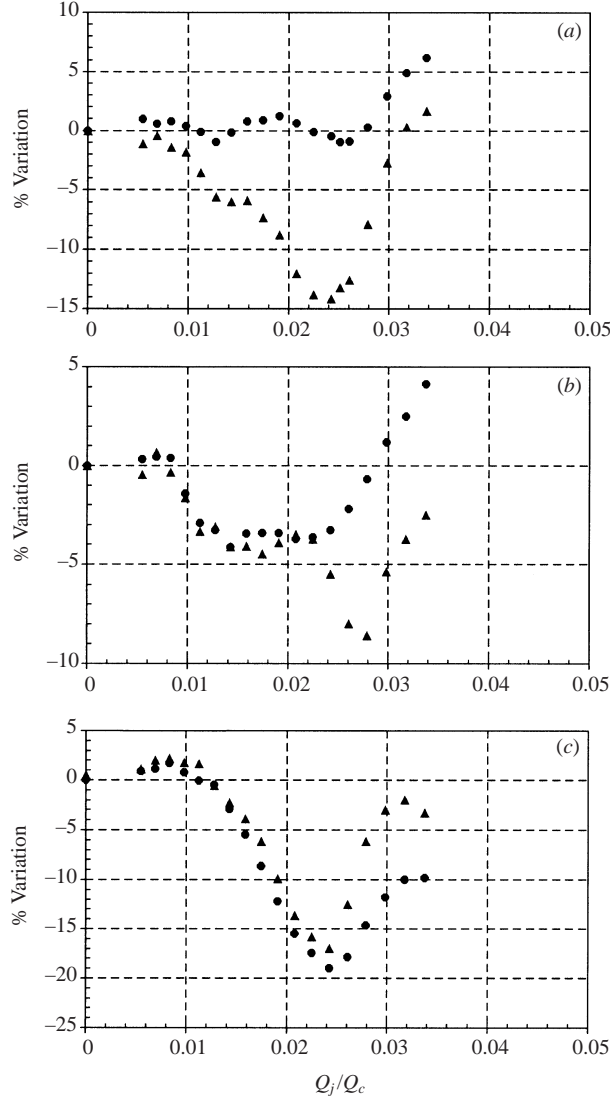
FIGURE 12. $\overline{C_f}$ (circles) and c'_f (triangles) variations as a function of mass flow rate at $x = 25H$ on the lower wall. (a) $z = 0$; (b) $z = 15\,\mathrm{mm}$; (c) $z = 30\,\mathrm{mm}$. $Re = 3600$.

friction reductions may be observed, see figure 12. On this wall maximum reductions of about 20% can be observed at $z = 30\,\mathrm{mm}$ (now in the up-flow region) for both mean value and fluctuation. Also, a very small $\overline{C_f}$ reduction, limited to a very narrow mass flow rate range, was obtained at $z = 0$. Differences in quantitative behaviour between the two walls are due to the fact that the vortical structures in our physical experiment are obviously not symmetrical (see e.g. figure 9c). No attempt has been made to optimize parameters like jet inclination or jet distance with the goal of obtaining a symmetrical control effect on the two walls.

In the following, most of the analysis will be performed on upper wall results, not only because the control is more effective there, but also because it can be considered representative of a turbulent boundary layer flow controlled by vortical structures generated by wall jets.
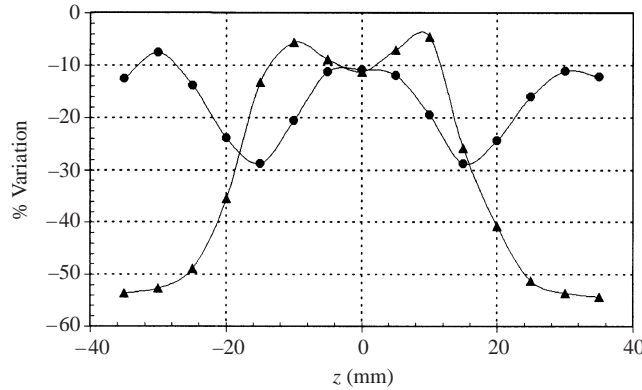
FIGURE 13. Spanwise distributions of $\overline{C_f}$ (circles) and c'_f (triangles) variations.
$Q_j/Q_c = 0.031$, $x/H = 25$, upper wall.
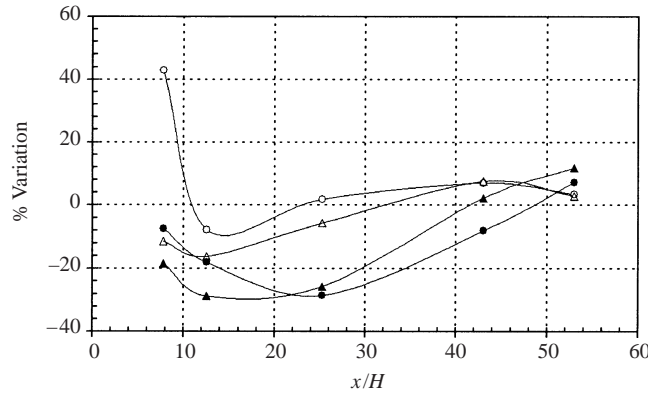
FIGURE 14. Streamwise distributions of $\overline{C_f}$ (circles) and c'_f (triangles) variations;
filled symbols: upper wall; open symbols: lower wall. $Q_j/Q_c = 0.031$, $z = 15$ mm.

Results in figure 11 and figure 12 confirm the numerical predictions of Schoppa & Hussain (1998), namely that the large-scale longitudinal vortices may produce skin friction and turbulence reductions and that these reductions occur for a small window of weak forcing flow. The control effect is negligible for weaker forcing, while stronger forcing leads to a drag increase, due to the disturbances introduced by the vortices (and, in the present experiment, by the jets).

Further details of the skin friction spanwise distribution are displayed in figure 13, where the spanwise distributions of percent variations of $\overline{C_f}$ and c'_f in the central region of the channel for the near-optimum conditions on the upper wall, $Q_j/Q_c = 0.031$ and $x = 25H$, are reported. Both quantities show a reduction along the whole channel span, but they exhibit different behaviours. The maximum skin friction reduction can be observed at about $z = \pm 15$ mm, in the cross-flow region. There is a reduction of the same order of magnitude ($\approx 30\%$) in c'_f at the same position, but the maximum reduction for this quantity is reached in the down-flow regions ($z = \pm 30$ mm) and attains a value as high as 55%. Note that at these positions the $\overline{C_f}$ reduction is of only approximately 10%.

The fact that the maximum reduction of the mean skin friction occurs at $z = \pm 15$ mm, i.e. exactly downstream of the position of the jet holes, may suggest that the observed reduction peaks might be a direct effect of jet blowing and possibly of

local flow separation rather than the effect of the vortical control, as is here claimed (in accordance with Schoppa & Hussain's 1998 prediction), at least as a dominant effect. In order to investigate this important point, the distribution of $\overline{C_f}$ and c_f' at $z = 15\,\text{mm}$ as a function of the distance from the jet holes was measured. Results from this test are reported in figure 14 for both the upper and the lower walls. From figure 14 the following arguments may be put forward:

(i) It is well known (Park & Choi 1999; Sumitani & Kasagi 1995; Yoshida *et al.* 1999) that a continuous uniform blowing decreases the skin friction while increasing the strength of the fluctuating quantities. In figure 14, conversely, both $\overline{C_f}$ and c_f' are clearly reduced by the manipulation. It will be shown in §3.2.2 that a similar reduction occurs also for the turbulent velocity fluctuation, at least in part of the explored flow field.

(ii) In the case of a near-wall flow manipulated by a jet blowing from a hole, it is expected that the skin friction is strongly reduced in the region just after the hole and then increases going downstream, towards its undisturbed value. In the present results, with reference to the upper wall, the $\overline{C_f}$ reduction is relatively small (about 7%) in a section 7.7 channel heights downstream of the jet, it takes a maximum value slightly lower than 30% at 25 channel heights and then increases towards values higher than the ones corresponding to the basic flow. Also note that, even though it was assumed that the whole friction reduction in the first measurement section ($X/H = 7.7$) was due to the blowing effect alone and that this would not reduce on going downstream, this effect would contribute less than 25% to the total reduction observed at the $x = 25H$ station.

(iii) The distributions of $\overline{C_f}$ and c_f' downstream of the jet section show similar behaviours on both channel walls, despite the fact that the jets originate from the upper wall only. This difference between the flow configurations on the two walls has the consequence that smaller reductions are present on the lower wall. Although it is not possible to rule out, based on the previous observation, that the flow at $x = 25H$ still keeps a memory of the direct jet blowing effect, the behaviour reported in figure 14 is consistent with the assumption that the main flow managing mechanism in the region $z = \pm 15\,\text{mm}$ is the vortical flow induced by VGJs. The idea that three-dimensional effects may reduce skin friction and turbulence is not new: in §1.2, analogous results obtained by transversally oscillating walls, rotating pipes and spanwise translation of the wall through a transversal belt mechanism were mentioned.

(iv) The observations from figures 9 and 10 and the behaviour of the velocity profiles (see figures 21 and 34) ensure that, in the measurement region, no separation is present on either wall.

(v) A further argument in favour of the assumption that the dominant mechanism influencing the flow is the forcing induced by the vortices rather than the direct action of the jets is provided by results presented in Appendix B. These results refer to a case in which the jets were alternately shut off, so that only parallel jets at a distance of 60 mm from each other were active. It can be seen (figure 38) that, for this geometry, the spanwise positions of the skin friction reduction peaks do not coincide with the jet exits.
More data will be presented in Appendix A for the lower wall, where the jets are not present.

The variations discussed until now are *local* variations of the mean and fluctuating components of the skin friction. In order to evaluate *global* results, values of $\overline{C_f}$ and c_f' averaged across the channel span have been computed. Following Schoppa & Hussain
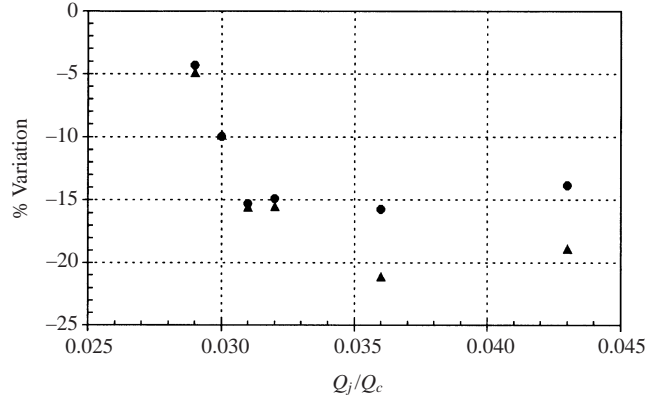
FIGURE 15. Spanwise-averaged $\overline{C_f}$ variations as a function of Q_j/Q_c. Triangles: integration across 'colliding jets' region. Circles: integration across 'counter-rotating streamwise vortices' region; $x = 25H$, upper wall.
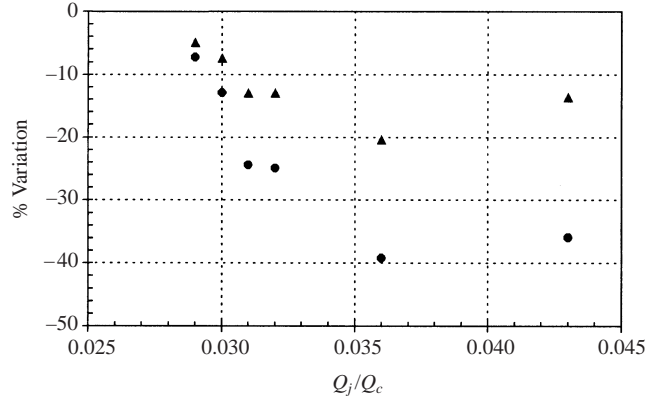
FIGURE 16. Spanwise-averaged c'_f variations as a function of Q_j/Q_c. Triangles: integration across 'colliding jets' region. Circles: integration across 'counter-rotating streamwise vortices' region; $x = 25H$, upper wall.

(1998), averages for the upper wall were computed both in the 'colliding z-directed wall jets region', extending from $z = -15\,\text{mm}$ to $z = 15\,\text{mm}$, and in the 'counter-rotating streamwise vortices region', i.e. from $z = -30\,\text{mm}$ to $z = 30\,\text{mm}$. Figures 15 and 16 show the averaged value of the mean skin friction and of the fluctuating component, respectively, as a function of the jet mass flow ratio at $x = 25H$ on the upper wall. The plot in figure 15 shows a reduction of approximately 15% in the value of $\overline{C_f}$ averaged over the 'counter-rotating streamwise vortices' region and a reduction with a maximum of 21% in the 'colliding z-directed wall jets' region. These reductions can be observed in the range $0.031 \leqslant Q_j/Q_c \leqslant 0.045$. The reduction in turbulent fluctuation reported in figure 16 shows maxima of 40% and 20% in the 'counter-rotating streamwise vortices region' and in the 'colliding z-directed wall jets region', respectively.

For their DNS simulation Schoppa & Hussain (1998) superimposed on a turbulent channel flow simulation a pair of counter-rotating vortices having the same scale as the ones used in the present experiment. For a perturbing flow considered as frozen and constant along the streamwise direction, having an optimized control
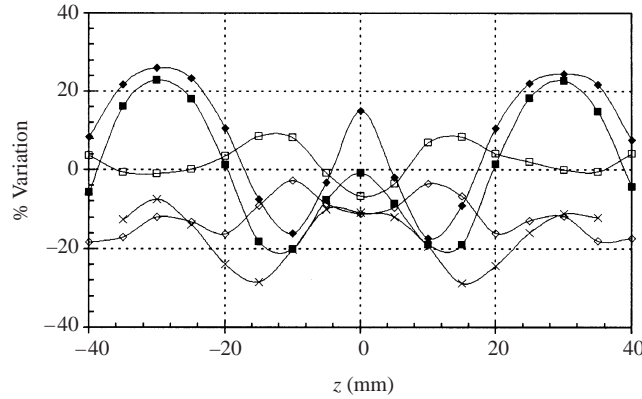
FIGURE 17. Spanwise distributions of $\overline{C_f}$ variations on the upper wall for various downstream stations. Filled diamonds: $x = 7.75H$; filled squares: $x = 12.5H$; crosses: $x = 25H$; open diamonds: $x = 43H$; open squares: $x = 53H$. $Q_j/Q_c = 0.031$.
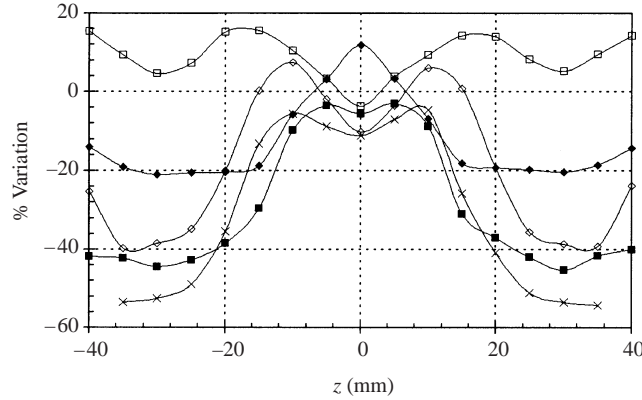
FIGURE 18. Spanwise distributions of c'_f variations on the upper wall for various downstream stations. Symbols as in figure 17; $Q_j/Q_c = 0.031$.

amplitude of 6% (i.e. $V_{\mathrm{con,max}} = 0.06V_C$), they showed a spanwise integrated skin friction reduction of 20% for imposed counter-rotating streamwise vortices and 50% for colliding z-directed wall jets. They attributed this drag reduction to the action of the forcing flow that significantly weakens the wall normal vorticity ω_y flanking lifted low-speed streaks, thereby preventing the streaks' sinuous instability which directly generates new streamwise vortices.

In the present experiment the strength of the forcing flow is obviously not uniform along the streamwise direction; it is thus of interest to look at the skin friction evolution along the channel, downstream of the jets. In figure 17, spanwise distributions of $\overline{C_f}$ on the upper wall for various sections downstream of the jets are shown for $Q_j/Q_c = 0.031$. Only in the $x = 25H$ and $x = 43H$ sections, where the vortical structures are properly developed, do skin friction reductions appear along the whole channel span. Closer to the jets, the effect of the disturbances locally produces an increase in $\overline{C_f}$, while downstream, at $x = 53H$, the flow tends to reach a skin friction value slightly higher than the one pertaining to the undisturbed flow. This is not surprising as, considering the increment in mass flow rate due to the jets, the asymptotic value of $\overline{C_f}$ that will be attained when canonical channel flow
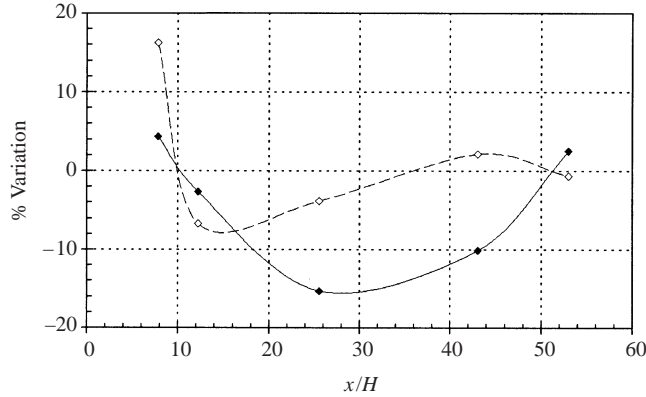
FIGURE 19. Streamwise distributions of spanwise-averaged $\overline{C_f}$ variations on the upper (filled symbols) and lower (open symbols) walls. $Q_j/Q_c = 0.031$.
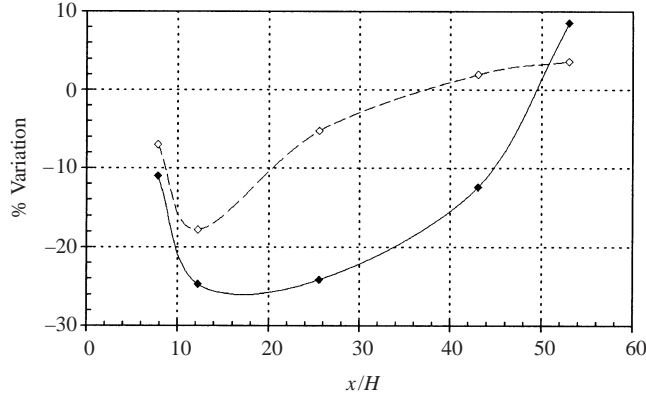
FIGURE 20. Streamwise distributions of spanwise-averaged c_f' variations on the upper (filled symbols) and lower (open symbols) walls. $Q_j/Q_c = 0.031$.

conditions are reached again is expected to be 5% higher than in the basic flow. Figure 18 shows how, surprisingly, the turbulent activity is already reduced in the near region immediately downstream the jets, and is kept lower than for the basic flow in the whole measurement region, with the exception of the last section, where it approaches the unmanipulated flow value.

Finally, figures 19 and 20 display the spanwise-averaged (across the 'counter-rotating streamwise vortices' region) values of $\overline{C_f}$ and c_f' as a function of the downstream distance from the jets, for the upper and lower walls. These figures confirm that the most favourable vortical flow conditions for reducing mean skin friction and turbulent activity are at $x = 25H$ and on the upper channel wall. In accordance with the aim of the present work, in the following all results will refer to the upper wall, at a downstream distance of $x = 25H$ and for $Q_j/Q_c = 0.031$. In Appendix A more results for the lower wall will be given.

3.2.2. *Velocity measurements*

Velocity profile measurements have been performed, for the manipulated flow at $x = 25H$ with $Q_j/Q_c = 0.031$, at $z = 0$, 15 mm and 30 mm; these positions are repre-
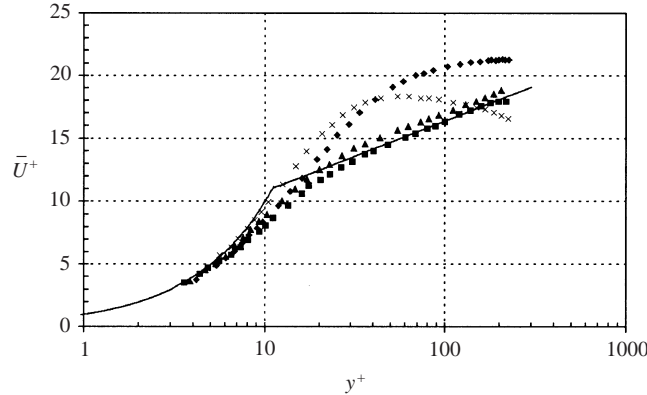
FIGURE 21. Mean velocity plots; solid line: law of the wall; squares: unmanipulated flow; triangles, diamonds, crosses: manipulated flow at $z = 0$, 15 mm and 30 mm, respectively. Upper wall, $x = 25H$, $Q_j/Q_c = 0.031$.

sentative of the up-flow, cross-flow and down-flow regions respectively. In figure 21 mean velocity profiles are reported on a semi-log plot; here all profiles are non-dimensionalized using the actual friction velocity of each case. The unmanipulated velocity profile and the standard law of the wall are also shown on the plot for comparison. The various profiles show a tendency to collapse onto a single curve in the viscous sublayer region, but are clearly shifted upwards in the logarithmic region, confirming that the skin friction is reduced by the action of the forcing flow. This indication is typical of most of the skin friction reducing flows (see e.g. Choi 1989). The up-flow region profile still exhibits a logarithmic region but with an higher value of the intercept constant in the logarithmic law of the wall. The logarithmic behaviour is, on the other hand, completely absent at $z = 15$ mm and at $z = 30$ mm.

The turbulent fluctuations of the streamwise velocity are presented in figure 22, where the root mean square of the velocity fluctuations is scaled with respect to the actual friction velocity. With this inner scaling, the behaviour of the manipulated channel flow appears to be similar, at $z = 0$, to that of the natural flow, while an increase in turbulence intensity, u'/u_τ, appears in the near-wall region ($y^+ \lesssim 70$) at $z = 15$ mm. A very strong u'/u_τ reduction is observed at $z = 30$ mm across most of the boundary layer: the peak value is decreased by 26% and a maximum reduction of 55% is found at $y^+ = 50$. Note that, in figure 22, u' is normalized with respect to the actual local friction velocity; nevertheless, when comparing non-normalized velocity fluctuations, turbulence reductions are found along the whole channel span for $y^+ \lesssim 100$.

Figure 21 clearly shows the substantial thickening of the viscous sublayer, that grows from $y^+ < 5$ for the canonical flow to values $y^+ > 10$ when controls are applied. In particular, at $z = 30$ mm, where the maximum fluctuation reduction (both for skin friction and near-wall velocity) is observed, the velocity profile appears to be tending towards a relaminarized condition. This thickening is also confirmed by the small shift of the fluctuation peak position towards higher values of y^+, see figure 22. A similar viscous sublayer thickening was observed in flows where skin friction reduction was obtained in various ways: manipulation by LEBU (see e.g. Savill & Mumford 1988; Iuso & Onorato 1995), spanwise oscillation of the wall (see e.g. Choi *et al.* 1998; Di Cicca *et al.* 2002*b*), compliant walls (see e.g. Lee, Fisher & Schwarz 1993), riblets (see e.g. Choi 1989). This viscous sublayer thickening is
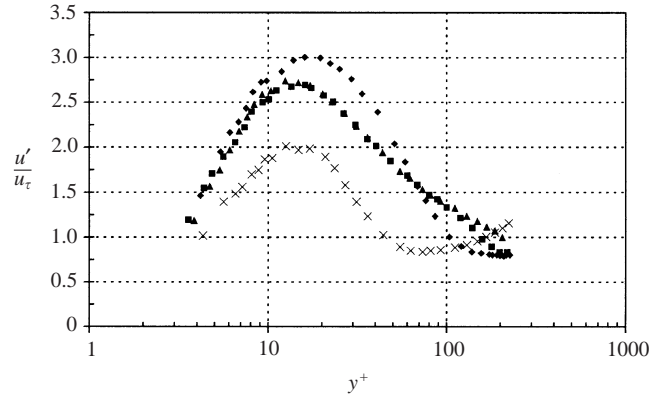
FIGURE 22. Fluctuating streamwise velocity component plots; squares: unmanipulated flow; triangles, diamonds, crosses: manipulated flow at $z = 0$, 15 mm and 30 mm, respectively. Upper wall, $x = 25H$, $Q_j/Q_c = 0.031$.
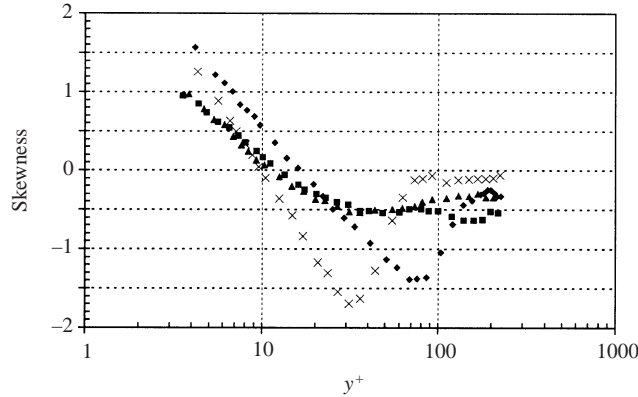
FIGURE 23. Velocity skewness distributions; squares: unmanipulated flow; triangles, diamonds, crosses: manipulated flow at $z = 0$, 15 mm and 30 mm, respectively. Upper wall, $x = 25H$, $Q_j/Q_c = 0.031$.

attributed to an adjustment of the balance between the turbulent energy production and the viscous dissipation, which reflects a reorganization of the turbulent structures, including an increase in the smallest eddy scale and a displacement of the turbulent events outward from the wall.

The velocity fluctuation skewness and flatness distributions are presented in figures 23 and 24. Both quantities appear to be increased by the flow manipulation in the near-wall region. The minimum for skewness and the maximum for flatness for $z = 15$ mm and $z = 30$ mm, respectively at $y^+ \approx 80$ and $y^+ \approx 30$, are related to the decrease of the channel shear flow thickness, as evidenced in figure 21. The higher-moment increases within the near-wall region are a consequence of the viscous sublayer thickness increase, as was already observed in several other friction reducing flows (see e.g. Baron & Quadrio 1996; Choi *et al.* 1998). The skewness and flatness increases are considered an indication of the growth of the wall structure scale.

4. Analysis and discussion

It has been shown that like a turbulent boundary layer, in a channel flow transversal jets from the wall, with appropriate inclination and mass flow rate, may produce
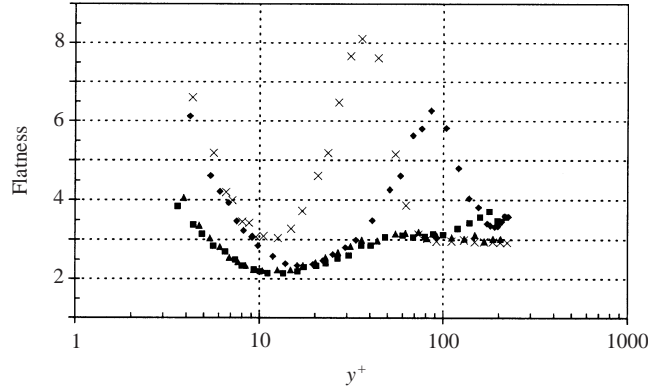
FIGURE 24. Velocity flatness distributions; squares: unmanipulated flow; triangles, diamonds, crosses: manipulated flow at $z = 0$, 15 mm and 30 mm, respectively. Upper wall, $x = 25H$, $Q_j/Q_c = 0.031$.

longitudinal vortices whose axes are located approximately on the channel symmetry plane. In the previous sections, an experimental demonstration has been provided that vortical forcing flows may reduce mean skin friction and near-wall turbulence. This agrees with results from Schoppa & Hussain's (1998) idealized numerical experiment. As in Schoppa & Hussain (1998), it was found that skin friction and turbulence reduction may be obtained only for a surprisingly weak forcing amplitude and that for an even weaker forcing the effect is negative or insignificant while a stronger forcing leads to increased skin friction and turbulence. Schoppa & Hussain (1998) postulated that the optimum control is attained when vortices are strong enough to stabilize the near-wall velocity streaks, yet weak enough not to introduce significant additional drag.

Also, it has been shown (see figure 11) that the optimum jet mass flow rate (and thus the optimum vortical flow strength) depends on the different flow regions in the spanwise direction and that the forcing flow produces different effects on the mean skin friction and on its turbulent component (figure 13). The maximum $\overline{C_f}$ reduction, for $Q_j/Q_c = 0.031$ and $x = 25H$, appears close to the maximum cross-flow position ($z \approx \pm 15$ mm), whereas the maximum turbulence reduction is observed in the down-flow region ($z \approx \pm 30$ mm), where mean skin friction reduction was found only in a very small range of Q_j/Q_c values (figure 11c). The different flow responses to the perturbation in the different regions suggests that there is not a single cause of the drag and turbulence variations.

It would be expected that any change in the main stress distribution (flow manipulation) may disturb the equilibrium state between the turbulence and the mean flow, leading to a reduction (or to an increase) in the ability of turbulence to extract energy from the mean flow. The reduction in turbulence production, particularly in the near-wall region, ultimately leads to a reduction in skin friction. For the flow discussed here, two perturbing causes can be identified, namely the momentum flux from and towards the wall (at $z \approx 0$ mm and $z \approx \pm 30$ mm respectively) and the three-dimensional disturbance (cross-flow) affecting most of the channel span. This behaviour is repeated along the z-axis. In the region close to the jets, a direct forcing from the jet blowing effect must also be expected.

The momentum transfer from and towards the wall characterizes boundary layers with blowing and suction, respectively. As reported in §1.2, blowing can decrease the skin friction and increase the turbulence intensity, while suction produces essentially
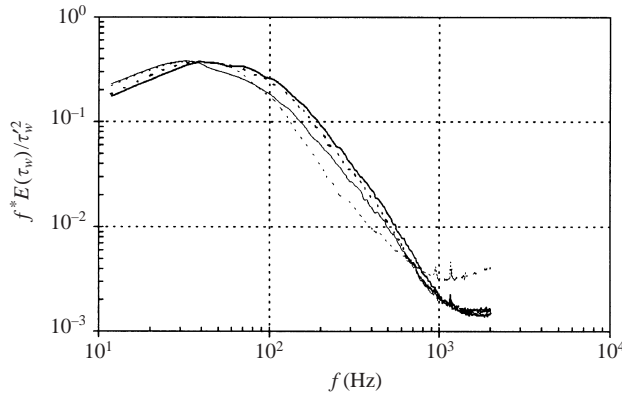
FIGURE 25. Skin friction power spectra. Thick solid line: unmanipulated case; thick broken line: manipulated, $z = 0$; thin solid line: manipulated, $z = 15\,\mathrm{mm}$; thin broken line: manipulated, $z = 30\,\mathrm{mm}$. Upper wall, $x = 25H$, $Q_j/Q_c = 0.031$.

opposite results. The effect of blowing in reducing mean skin friction may be directly attributed to the fact that the near-wall high-shear-rate layers are moved farther from the wall, thus modifying the wall vorticity evolution and probably weakening the source for new streamwise vortices. Moreover these streamwise vortices, being pushed away from the wall, are less effective in inducing high values of wall shear stress. The effect of suction in reducing turbulence is attributed by various authors to a stabilization of the velocity streaks (see § 1.2).

Three-dimensional effects on the turbulence structure have been the object of several studies. As shown in § 1.2, superposing a cross-flow over a canonical turbulent boundary layer was found by different authors to cause both skin friction and turbulence reduction. Most of these authors attribute the turbulence (and hence shear stress) reduction to the weakening and stabilizing action of the cross-flow on the low-speed streaks.

The correspondence between such flows and the manipulated channel flow discussed in the present paper supports the concept that the benefits obtained in skin friction and turbulence reduction can be attributed largely to the management of an important link in the feedback mechanism which normally sustains the wall turbulence, namely to a stabilizing action on the low-speed streaks. Some evidence supporting this statement will be analysed in the following.

In order to examine modifications in the wall turbulence scales, spectra of both skin friction and velocity fluctuation signals, at $y^+ \approx 15$, were computed. In figures 25 and 26 the power spectral density of τ_w and u is multiplied by the frequency and divided by the actual variance, so that the distributions' peaks are centred about the most energetic frequencies. Both plots show a shift in the peak frequency and in the whole spectrum towards lower frequencies for the manipulated flow; the maximum shift was obtained for $z = 15\,\mathrm{mm}$. This can be interpreted as a manifestation of an increase in the length of the velocity streaks, i.e. an increment in longitudinal coherence which may be considered a consequence of an increased stability caused by the forcing flow control. Moreover, an increase in temporal scale is confirmed by the τ_w and u (at the same position as for the spectra) autocorrelation functions reported in figures 27 and 28. Choi, *et al.* (1998), for an oscillating wall, found that the low-speed streaks duration was increased by a factor 4 when the oscillation was at optimum conditions.
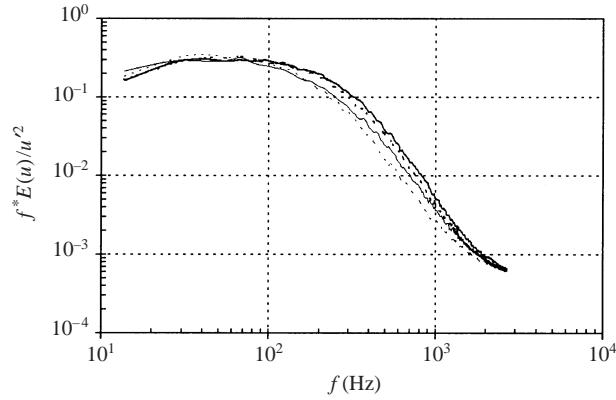
FIGURE 26. Velocity power spectra at $y^+ \approx 15$. Thick solid line: unmanipulated case; thick broken line: manipulated, $z = 0$; thin solid line: manipulated, $z = 15\,\text{mm}$; thin broken line: manipulated, $z = 30\,\text{mm}$. Upper wall, $x = 25H$, $Q_j/Q_c = 0.031$.
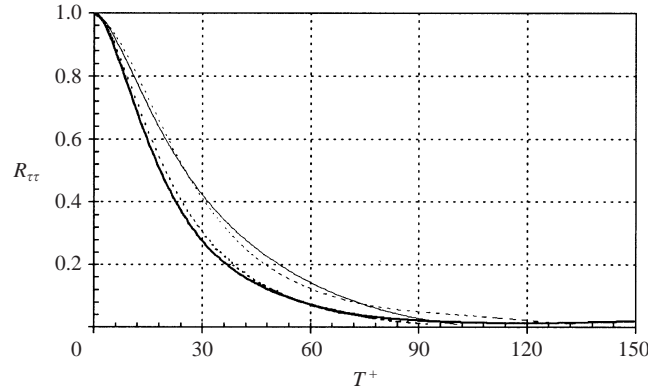
FIGURE 27. Skin friction autocorrelation functions. Thick solid line: unmanipulated case; thick broken line: manipulated, $z = 0$; thin solid line: manipulated, $z = 15\,\text{mm}$; thin broken line: manipulated, $z = 30\,\text{mm}$. Upper wall, $x = 25H$, $Q_j/Q_c = 0.031$.

Flack (1997), investigating the effect on the near-wall structures of increased three-dimensionality by hydrogen bubble visualization, found that cross-flows stabilize the near-wall structure, producing a more quiescent near-wall region, in particular with fewer burst events. In order to check this aspect in the flow discussed here, skin friction signals were analysed by searching for events where the local (short-time averaged) variance exceeds the total signal variance multiplied by a threshold constant K (Shah & Antonia 1987). Only events characterized by $d\tau_w/dt > 0$ at the detection instant were considered. Such wall events represent the 'signature' of the near-wall bursts. In figure 29 the frequency of occurrence of such events as a function of the threshold constant is shown. The frequency f^+ is scaled with respect to the unmanipulated case inner variables; the short integration time, T, is 13 times the viscous scale time of the basic flow. To find such events, the local variance was compared to K times the global variance of the same signal. In figure 30 f^+ is plotted against T^+ for $K = 1$. The plots in figures 29 and 30 clearly show that, for all the short integration times T^+ and the threshold constants K examined the number of burst events is reduced by the manipulation in all regions, in particular in the down-flow region, where the largest turbulence reduction is also observed.
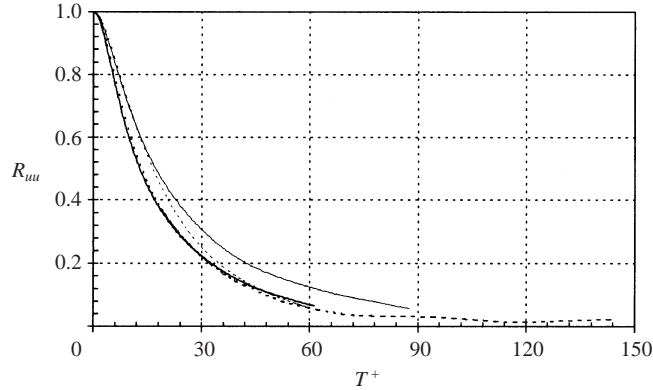
FIGURE 28. Velocity autocorrelation functions. Thick solid line: unmanipulated case; thick broken line: manipulated, $z = 0$; thin solid line: manipulated, $z = 15$ mm; thin broken line: manipulated, $z = 30$ mm. Upper wall, $x = 25H$, $Q_j/Q_c = 0.031$.
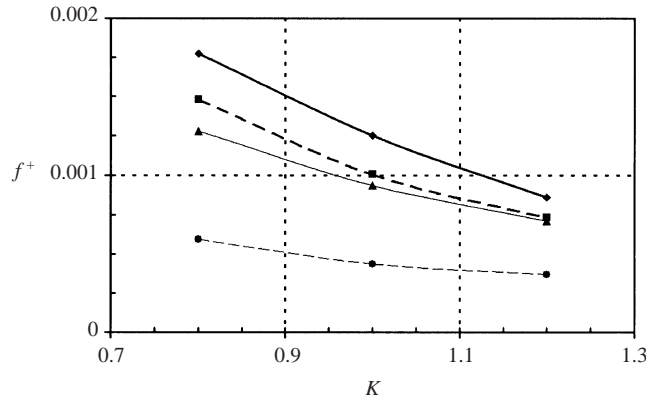
FIGURE 29. Wall skin friction burst frequency as a function of the threshold constant K. Thick solid line: unmanipulated case; thick broken line: manipulated, $z = 0$; thin solid line: manipulated, $z = 15$ mm; thin broken line: manipulated, $z = 30$ mm. $T^+ = 13$. Upper wall, $x = 25H$, $Q_j/Q_c = 0.031$.

The burst signature was then conditionally sampled on the events detected for $T^+ = 13$ and $K = 1$ and ensemble averaged, providing the results shown in figure 31. The ensemble-averaged skin friction $\langle \tau_w \rangle$ is normalized with respect to the skin friction standard deviation τ'_w in the natural (non-manipulated) flow case. A reduction in slope around $t = 0$ is evident (and even more so in the central region zoom of figure 31b), showing that burst events occurring in the manipulated flow case are both weaker and less frequent. Again, the position where the effect is most evident is $z \approx \pm 30$ mm, where the burst amplitude $\langle \tau_W \rangle$ is also reduced.

Considering now that this burst signature is associated with a strong down-wash of high-momentum fluid towards the wall produced by the near-wall longitudinal vortices, the results of figure 31 are consistent with the argument that the forcing flow reduces the near-wall longitudinal vortices regeneration process, presumably by weakening (and thus stabilizing) the low-speed streaks.

An additional connection between the present pointwise flow measurements and the near-wall turbulent structures can be seen in figure 32, where probability density
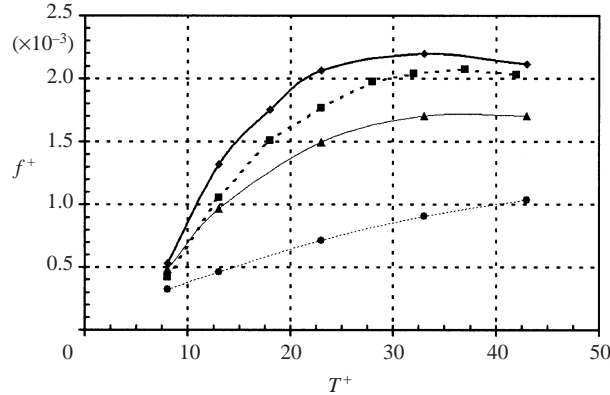
FIGURE 30. Wall skin friction burst frequency as a function of the short integration time T^+. Thick solid line: unmanipulated case; thick broken line: manipulated, $z = 0$; thin solid line: manipulated, $z = 15$ mm; thin broken line: manipulated, $z = 30$ mm. $K = 1$. Upper wall, $x = 25H$, $Q_j/Q_c = 0.031$.

functions (PDFs) of the fluctuating velocity component time derivatives, at $y^+ \approx 15$, in the various regions are reported. Velocity time derivatives were normalized with respect to the value of the standard deviation in the basic flow. By looking first at the canonical flow, the high positive skewing of $\mathrm{d}u/\mathrm{d}t$ was attributed by Onorato & Iuso (2001) to the wavy nature (and to the wavy motion) of the low-speed streaks in the plane parallel to the wall. Indeed, as was shown by Schoppa & Hussain (1998), when a yawed low-speed streak passes over a probe, a sharper velocity gradient must be expected when going from the low-speed region to the high-speed region ($\mathrm{d}u/\mathrm{d}t > 0$) than in the opposite case ($\mathrm{d}u/\mathrm{d}t < 0$). Now this asymmetry in the PDFs is less evident for the manipulated flow, particularly in the down-flow region, $z \approx \pm 30$ mm. Again, this result may be rationally interpreted by assuming that the meandering motion of the streaks was reduced by the forcing flow and the streaks themselves are consequently less unstable. Moreover, it is significant that the negative values of $\mathrm{d}u/\mathrm{d}t$ also appear to be reduced in the manipulated flow case compared to the canonical flow. Indeed, according to Schoppa & Hussain (1998), vortex stretching associated with high positive values of $\mathrm{d}u/\mathrm{d}x$ (i.e. negative values of $\mathrm{d}u/\mathrm{d}t$) is of some importance in the process by which the coherent vortices are generated.

In figure 33, the data of figure 32 were rescaled by normalizing the velocity time derivatives with respect to the actual root mean square values for each case. This scaling shows the intermittent characteristics of the flow fields in the different regions, with and without manipulation; the corresponding values of skewness and flatness are also reported. It is clear that the manipulated flow is more intermittent than when VGJs are off. In particular, for $z = 30$ mm (down-flow region), where the maximum turbulent fluctuations reduction is obtained, the intermittency is the highest; the flatness value is more than twice that of the unmanipulated flow. It has already been observed that the manipulation is responsible for an increase in the streamwise size of the wall structures and for a reduced frequency of the wall burst events. The increased intermittency can thus be connected to the fact that the high-time-derivative locations are more dispersed throughout the flow field.

Some of the results discussed here, like the increment in longitudinal scale, the decrease in the frequency of bursting events and the modification in greater symmetry of the $\mathrm{d}u/\mathrm{d}t$ PDFs have been interpreted as a manifestation of the fact that the low-speed streaks have been weakened by the forcing flow. Consequently, according to
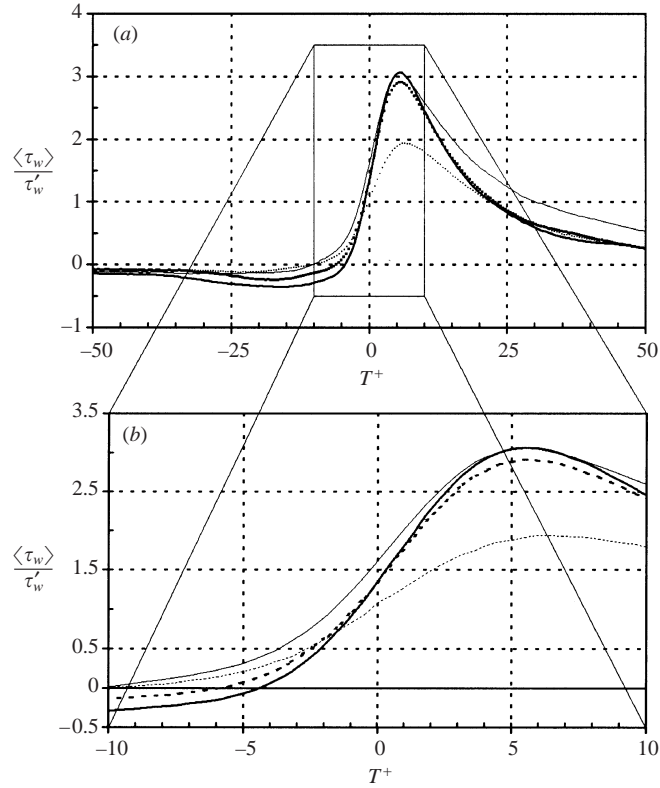
FIGURE 31. (*a*) Conditionally sampled burst of wall skin friction fluctuations. Thick solid line: unmanipulated case; thick broken line: manipulated, $z = 0$; thin solid line: manipulated, $z = 15\,\text{mm}$; thin broken line: manipulated, $z = 30\,\text{mm}$. $K = 1$; $T^+ = 13$. Upper wall, $x = 25H$, $Q_j/Q_c = 0.031$. (*b*) Zoom of the central region.
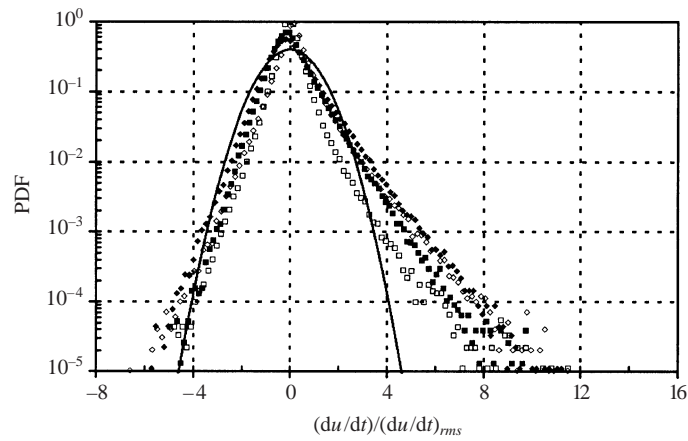
FIGURE 32. Probability density functions for the fluctuating velocity time-derivatives at $y^+ \approx 15$. Thick solid line: reference Gaussian curve; filled diamonds: unmanipulated case data; filled squares: manipulated case data, $z = 0$; open diamonds: manipulated case data, $z = 15\,\text{mm}$; open squares: manipulated case data, $z = 30\,\text{mm}$. Normalization with respect to the unmanipulated case. Upper wall, $x = 25H$, $Q_j/Q_c = 0.031$.
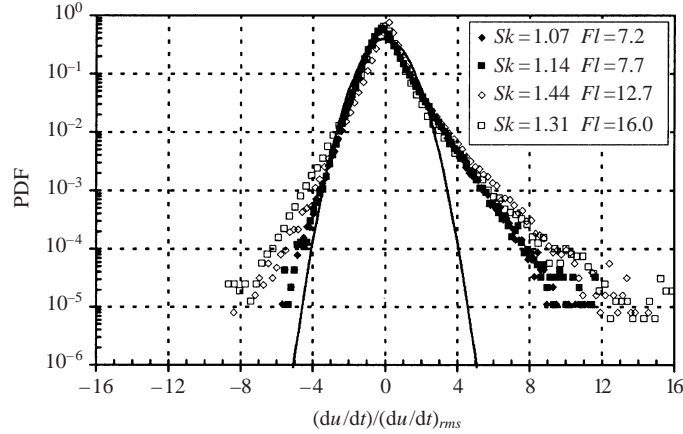
FIGURE 33. Probability density functions for the fluctuating velocity time-derivatives. Thick solid line: reference Gaussian curve; filled diamonds: unmanipulated case data; filled squares: manipulated case data, $z = 0$; open diamonds: manipulated case data, $z = 15\,\text{mm}$; open squares: manipulated case data, $z = 30\,\text{mm}$. Normalization with respect to the actual case. Upper wall, $x = 25H$, $Q_j/Q_c = 0.031$.

findings in the literature, being partly stabilized, the velocity streaks are less efficient in the turbulence reproduction cycle (see e.g. Jeong *et al.* 1997; Jimenez & Pinelli 1997, 1998).

In order to show that the present form of flow manipulation also increases the turbulence lateral scale (and presumably the mean spacing of the low-speed streaks) and to further show that the forcing vortical structures actually have a weakening action on the velocity streaks, selected results from a parallel experiment conducted in a turbulent boundary layer flow, also manipulated through embedded longitudinal large-scale vortices, is reported in Appendix C.

5. Summary and conclusions

By introducing into a channel flow an array of transversal, inclined, small jets, a marked reduction in turbulence and wall shear stress was observed downstream of the injection section despite the large amount of noise introduced into the flow. The decrease in fluctuations and skin friction is attributed mainly to the action of the flow induced by the jet-generated series of counter-rotating vortex pairs, whose axes are located approximately at the channel centreplane. Mean skin friction reductions as high as 30% were observed in the regions where a cross-flow develops and skin friction fluctuation reductions larger than 50% were measured where the flow induced by the vortices is directed towards the wall. Mean and fluctuating skin friction, averaged across the whole channel span, were decreased by 15% and 40%, respectively. These high values of skin friction and turbulence reduction have been measured on the channel upper wall (where the VGJs are operated) and in the section where optimal flow manipulation conditions were obtained. Data on the opposite channel wall show a similar near-wall behaviour, but with lower overall wall friction and turbulence reductions. The decreased effectiveness of longitudinal vortices in reducing skin friction and turbulence on the lower wall is due to the asymmetric structure of the perturbing flow and to the fact that the jets mass flow rate was optimized by looking at the upper wall only; these aspects are at present being investigated.

The main physical alterations detected in the flow due to this large-scale manipulation are the substantial thickening of the viscous sublayer, an increase in the longitudinal coherence of the near-wall velocity streaks and an increase of their mean lateral spacing (see Appendix C), a marked reduction of the burst event frequency and strength, and a modification of the symmetry of the du/dt PDFs, demonstrating a weakening of the fluctuating velocity gradients. It also seems clear that in the manipulated case the velocity and wall shear stress time derivatives are characterized by an increased intermittency. This has also been attributed to an increase in the coherence of the longitudinal structures and to a reduction in the wall burst event frequency.

All such alterations could be interpreted as the consequence of the weakening action of the forcing flow on the low-speed structures, which then become more stable and less efficient in generating new longitudinal vortices and, finally, in regenerating turbulent energy.

In the present paper the turbulence reduction was explained through explicit reference to the turbulence regeneration mechanism based on the instability of the low-speed streaks. However, as mentioned in the introduction, this is not the only observed regeneration mechanism. The present authors are convinced that the wall cycle, demonstrated experimentally and numerically in several other studies (some of which are listed in the introduction), is also active in the near-wall turbulence reproduction. More precisely, the present authors are in agreement with Jimenez & Pinelli (1999) that in real flows there is competition amongst different turbulence reproduction mechanisms and that one mechanism may overcome another according to the local flow parameters, which might include the Reynolds number. The subject is still open and at present far from being fully understood. The main reason why in the present paper attention was focused essentially on the vortex-free streak cycle is the correspondence between the manipulation technique applied here and the flow control operated through suction/blowing and cross-flow. In both cases, several authors (cited in the introduction) have attributed the turbulence reductions to the stabilization of the velocity streaks.

It should be emphasized that the purpose of this investigation was not limited to the possible technological applications; its aim was rather to promote a better understanding of wall turbulent shear flows and their response to external forcings. Moreover, work is in progress in the interesting direction of increasing the distance between the jets and thus the scale of the forcing vortical flow. Encouraging results have been already obtained for longitudinal vortices located more than 1000 viscous length-scales apart. A preliminary result is reported in Appendix B.

A clear finding of some relevance for possible technological applications is that local friction drag and turbulence reduction occurs only for a relatively small range of the vortical flow strength. Furthermore, in a real flow optimum conditions depend on the vortex development in the streamwise direction.

Finally, it should be acknowledged that no attempt has been made to optimize the system, taking into account the penalties for collecting, ducting and injecting the VGJ flow; these penalties were not evaluated.
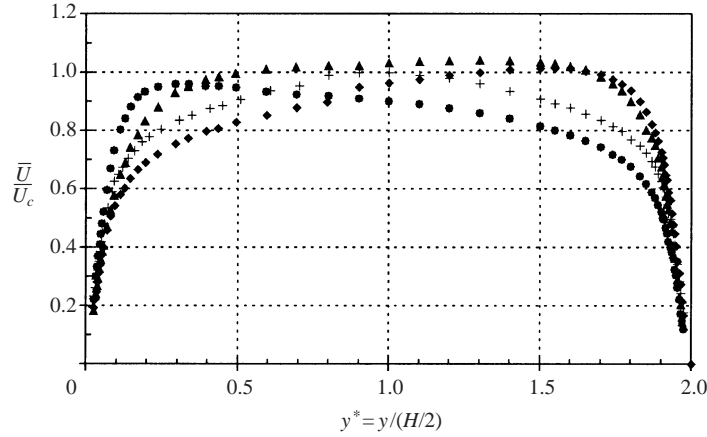
FIGURE 34. Complete streamwise velocity profiles. Crosses: unmanipulated case data; diamonds: manipulated case data, $z = 0$; triangles: manipulated case data, $z = 15$ mm; circles: manipulated case data, $z = 30$ mm. $x = 25H$, $Q_j/Q_c = 0.031$.

Appendix A. Additional data

For the sake of completeness, in this Appendix additional measurements for $Q_j/Q_c = 0.031$ are presented. Only summary comments are provided.

In figure 34 the mean velocity distribution at $x = 25H$, scaled with the unmanipulated case centreline velocity, throughout the channel section is reported; the jets are injected from the wall corresponding to $y = 0$; lengths are scaled with the channel half-height. It is interesting to compare the velocity distributions in the various spanwise positions with the unmanipulated case, which obviously exhibits a symmetrical behaviour. Data referring to the manipulated case indicate lower values of the near-wall velocity derivatives at the upper wall ($y = 0$), where larger skin friction reductions were observed. The behaviour of the profiles at $z = 0$ mm and $z = 30$ mm is consistent with the fact that when there is up-flow on one wall, there is down-flow on the other one and vice versa. In figure 35 the root mean square of the velocity fluctuations is displayed. Close to the two walls a clear reduction in turbulence is observable; this is more marked in the proximity of the upper wall ($y = 0$).

Figures 17 and 18 displayed the distribution on the upper wall of $\overline{C_f}$ and c'_f for various downstream stations; figures 36 and 37 report the behaviour of the same quantities at the same stations on the lower wall (opposite to the jets). A skin friction reduction can be seen in the up-flow (now located at $z = 30$ mm) region at the first three measurement stations, and in the cross-flow region at the $x = 12.5H$ and $x = 25H$ stations. No reduction is observed in the down-flow region for $Q_j/Q_c = 0.031$. It was shown in figure 12 that drag reduction is present on the lower wall in the down-flow region only for a small range of mass flow rates, in the vicinity of $Q_j/Q_c = 0.021$. Figure 37 shows that turbulence reduction is achieved along the whole channel span for $x = 7.75H$ and $x = 25H$.

Appendix B. Increased lateral scale of vortices

Increasing the lateral scale of the longitudinal vortices has been attempted by switching off the vortex generator jets alternately. With reference to figure 2, the
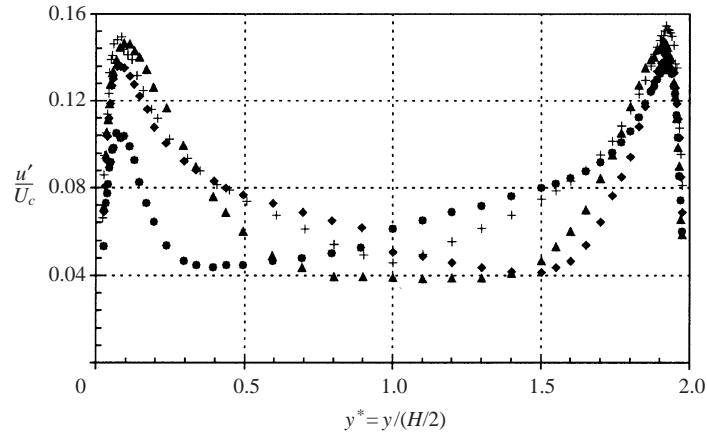
FIGURE 35. Complete streamwise velocity fluctuating component profiles. Crosses: unmanipulated case data; diamonds: manipulated case data, $z = 0$; triangles: manipulated case data, $z = 15$ mm; circles: manipulated case data, $z = 30$ mm. $x = 25H$, $Q_j/Q_c = 0.031$.
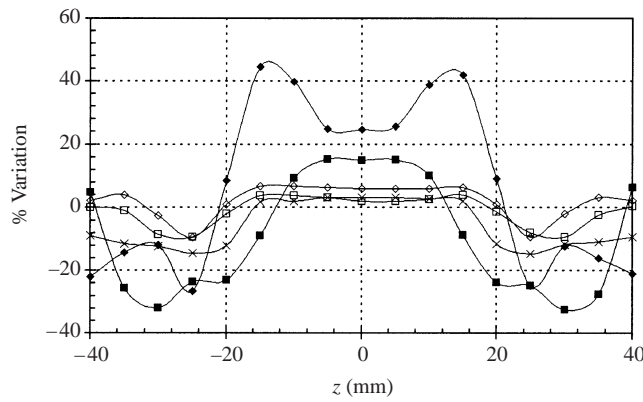
FIGURE 36. Spanwise distributions of $\overline{C_f}$ variations on the lower wall for various downstream stations. Filled diamonds: $x = 7.75H$; filled squares: $x = 12.5H$; crosses: $x = 25H$; open diamonds: $x = 43H$; open squares: $x = 53H$. $Q_j/Q_c = 0.031$.
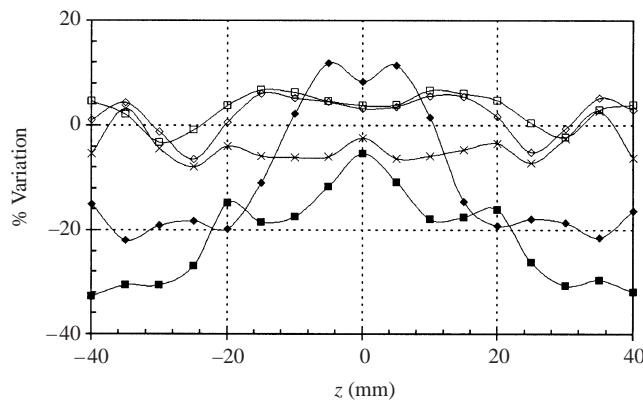
FIGURE 37. Spanwise distributions of c_f' variations on the lower wall for various downstream stations. Symbols as in figure 17; $Q_j/Q_c = 0.031$.
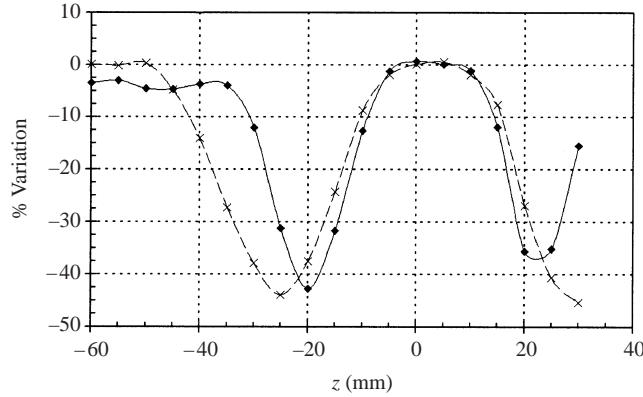
FIGURE 38. Spanwise distribution of $\overline{C_f}$ (diamonds, full line) and c'_f (crosses, broken line) variations with jets alternately off. $Q_j/Q_c = 0.031$, $x = 25H$, upper wall.

distance between the jets was modified to 60 mm (i.e. more than 1000 wall units) and the jets were all oriented in the same spanwise direction. The vortices produced in this way are no longer counter-rotating. The resulting flow modifications at $x = 25H$ for a jet mass flow rate $Q_j/Q_c = 0.031$ are summarized in figure 38, in which the reductions in $\overline{C_f}$ and c'_f thus obtained are reported. The strong reductions of both quantities, which reach values of the order of 40% at their respective peaks, are impressive.

Observe, with reference to the discussion in §3.2.1 about the direct action of the jets on skin friction reduction, that in this configuration the peaks of reduction are no longer aligned with the jets locations, which are now situated at $z = +15$ mm and $z = -45$ mm.

Appendix C. A flat-plate turbulent boundary layer

In parallel with the experiments described in this paper, a companion experiment was conducted on a flat-plate turbulent boundary layer, manipulated by large-scale longitudinal vortices. In order to support some of the conclusions in §4, a few results from the companion experiment are reported in this Appendix. The complete description of the experiment and full results are given in Di Cicca *et al.* (2002*a*). The jet configuration in this experiment was the same as described in figure 2, except that only one wall was present, again providing a spacing of about 500 wall units between the vortices. The ratio of the jet mass flow to the boundary layer mass flow was about one order of magnitude lower than in the channel experiment. The working fluid was water and the natural boundary layer, at the injection section, was characterized by $Re_\theta = 1160$, $H = 1.32$, $u_\tau/U_e = 0.052$ and $\delta = 37$ mm. Digital particle image velocimetry (DPIV) was used as a diagnostic tool, while no direct measurement of skin friction was attempted. In figure 39 rear views of the mean cross-flow field at $x = 130$ mm and $x = 250$ mm (i.e. approximately 3.5 and 7 boundary layer heights downstream of the jets) are displayed; the wall is identified by $y = 0$. It can be clearly seen that the central pair of counter-rotating vortices is fully immersed in the boundary layer. The previously described up-flow, down-flow and cross-flow regions are now clearly and quantitatively observable. The maximum cross-flow velocity due to the forcing flow is less than 3% of the external velocity at $x = 250$ mm. When compared to the natural boundary layer, a mean velocity reduction in the buffer layer
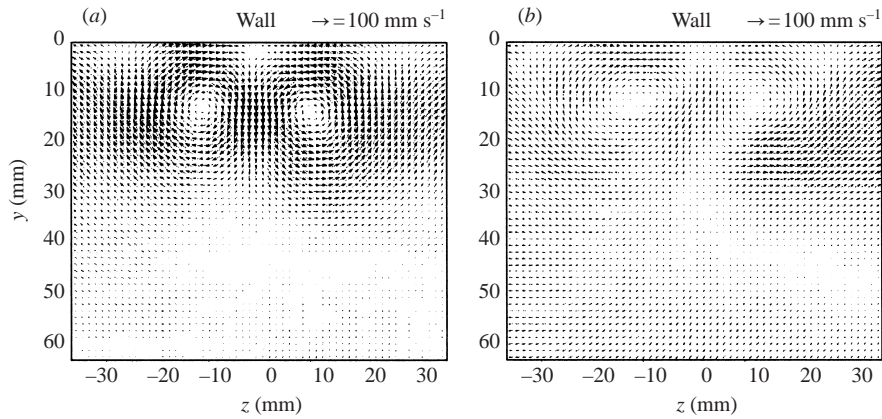
FIGURE 39. Mean velocity flow field in the cross-planes (y, z) at $x = 130\,\text{mm}$ (a)
and $x = 250\,\text{mm}$ (b).
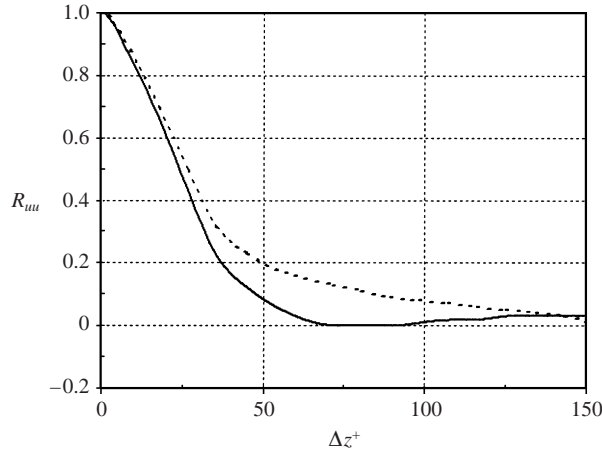
FIGURE 40. Spanwise correlation functions R_{uu} at $y^+ = 20$. Solid line: natural boundary layer;
broken line: manipulated boundary layer.

was measured in the region between vortex axes at $x = 250\,\text{mm}$, with a maximum reduction of 13% at $z = 0$ and $y^+ = 20$. Turbulence reduction was observed close to the wall, with a maximum value of 18% in the up-flow region, in correspondence to the u' distribution peak ($y^+ \approx 15$).

The main reason for reporting these DPIV results here is to show the next two figures, in which measurements in a plane parallel to the wall at $y^+ \approx 20$ (maximum turbulence reduction region) are reported for $x = 250\,\text{mm}$.

In figure 40 the spanwise correlation functions R_{uu} of the longitudinal fluctuating velocity component for the natural and the manipulated boundary layers are reported. Lengths are scaled with respect to the viscous length corresponding to the natural case. An increase in lateral scale produced by the forcing flow is evident. This presumably means that the flow control increases the mean spacing of the low-speed streaks; consequently, a wider mean spacing may be expected between the quasi-longitudinal boundary layer vortical structures inducing the velocity streaks; this could be associated with local friction drag and turbulence reductions.
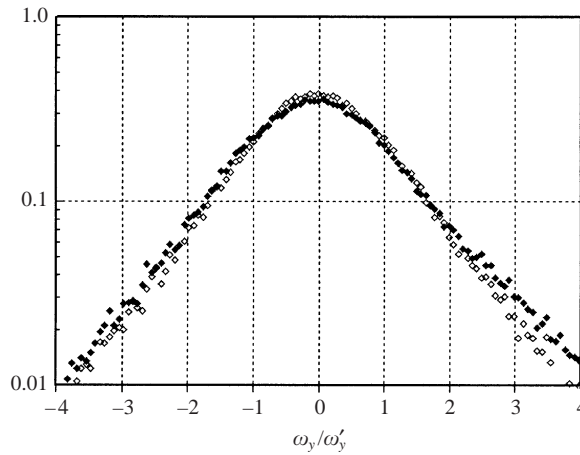
FIGURE 41. Probability density functions of wall normal vorticity. Filled diamonds: natural boundary layer; open diamonds: manipulated boundary layer.

In figure 41 the probability density functions of the wall-normal vorticity, ω_y (note that this quantity essentially coincides with $\partial u/\partial z$), in the plane $y^+ = 20$ are compared for the natural and the manipulated boundary layers. Vorticity is normalized with respect to the root mean square value of the natural flow vorticity, ω_y'. The comparison shows that the PDF tails, for ω_y values higher than ω_y' and lower than $-\omega_y'$, assume values which are slightly lower in the case of manipulated flow. This behaviour may be interpreted as the consequence of a possible weakening action of the forcing flow on the velocity streaks.

The conclusion that can be drawn from this Appendix is that embedded large-scale longitudinal vortices may reduce skin friction and turbulence in a turbulent boundary layer also and that this reductions can be associated with an increase in the turbulence lateral scale and to a weakening of the low-speed streaks.

REFERENCES

ADRIAN, R. J., MEINHART, C. D. & TOMKINS, C. D. 2000 Vortex organization in the outer region of the turbulent boundary layer. *J. Fluid Mech.* **424**, 1–54.

ALFREDSSON, P. H., JOHANSSON, A. V., HARITODINIS, J. H. & ECKELMANN, H. 1988 The fluctuating wall-shear stress and the velocity field in the viscous sublayer. *Phys. Fluids* **31**, 1026–1033.

ANTONIA, R. A., FULACHIER, L., KRISHNAMOORTHY, L. V., BENABID, T. & ANSELMET, F. 1988 Influence of wall suction on the organized motion in a turbulent boundary layer. *J. Fluid Mech.* **190**, 217–240.

BARON, A. & QUADRIO, M. 1996 Turbulent drag reduction by spanwise wall oscillations. *Appl. Sci. Res.* **55**, 311–326.

BERNARD, P. S. & WALLACE, J. M. 1997 Vortex kinematics, dynamics, and turbulent momentum transport in wall bounded flows. In *Self-Sustaining Mechanisms of Wall Turbulence* (ed. R. L. Panton). Advances in Fluid Mechanics, vol. 15, pp. 65–81. Southampton, UK: Computational Mechanics Publications.

BLACKWELDER, R. & ECKELMANN, H. 1979 Streamwise vortices associated with the bursting phenomenon. *J. Fluid Mech.* **94**, 577–594.

BLACKWELDER, R. F. & HARITODINIS, J. H. 1983 Scaling of the bursting frequency in turbulent boundary layers. *J. Fluid Mech.* **132**, 87–103.

CHOI, K. S. 1989 Near-wall structure of a turbulent boundary layer with riblets. *J. Fluid Mech.* **208**, 417–458.

CHOI, K. S. 2000 European drag reduction – research recent developments and current status. *Fluid Dyn. Res.* **26**, 325–335.

CHOI, K. S., DEBISSCHOP, J. R. & CLAYTON, B. R. 1998 Turbulent boundary layer control by means of spanwise wall oscillations. *AIAA J.* **36**, 1157–1163.

DI CICCA, G. M., IUSO, G., SPAZZINI, P. G. & ONORATO, M. 2002a A PIV study of the influence of large scale streamwise vortices on a turbulent boundary layer. Accepted for publication in *Exps. Fluids*.

DI CICCA, G. M., IUSO, G., SPAZZINI, P. G. & ONORATO, M. 2002b Particle image velocimetry investigation of turbulent boundary layer manipulated by spanwise wall oscillations. *J. Fluid Mech.* **467**, 41–56.

DI CICCA, G. M., ONORATO, M., IUSO, G., BOLLITO, A. & SPAZZINI, P. 1999 DPIV study of a non canonical boundary layer flow. In *Proc. 3rd Intl Workshop in Particle Image Velocimetry, Santa Barbara, CA, USA* (ed. R. Adrian, Y. Hassan & C. Meinhart).

FLACK, K. A. 1997 Near-wall structure of three-dimensional turbulent boundary layers. *Exps. Fluids* **23**, 335–340.

GAD-EL HAK, M. 2000 *Flow Control – Passive, Active, and Reactive Flow Management*. Cambridge University Press.

HAMILTON, J. M., KIM, J. & WALEFFE, F. 1995 Regeneration mechanisms of near-wall turbulence structures. *J. Fluid Mech.* **287**, 317–348.

HANRATTY, T. J. & PAPAVASSILIOU, D. V. 1997 The role of wall vortices in producing turbulence. In *Self-Sustaining Mechanisms of Wall Turbulence* (ed. R. L. Panton). Advances in Fluid Mechanics, vol. 15, pp. 83–108. Southampton, UK: Computational Mechanics Publications.

IUSO, G. & ONORATO, M. 1995 Turbulent boundary layer manipulation by outer layer devices. *Meccanica* **30**, 359–376.

JEONG, J., HUSSAIN, F., SCHOPPA, W. & KIM, J. 1997 Coherent structures near the wall in a turbulent channel flow. *J. Fluid Mech.* **332**, 185–214.

JIMENEZ, J. & MOIN, P. 1991 The minimal flow unit in near wall turbulence. *J. Fluid Mech.* **225**, 221–240.

JIMENEZ, J. & PINELLI, A. 1997 Wall turbulence: how it works and how to damp it. *AIAA Paper* 97-2112.

JIMENEZ, J. & PINELLI, A. 1998 The role of coherent structure interactions in the regeneration of wall turbulence. *Advances in Turbulence*, vol. 7, pp. 155–158. Kluwer.

JIMENEZ, J. & PINELLI, A. 1999 The autonomous cycle of near-wall turbulence. *J. Fluid Mech.* **389**, 335–359.

JOHNSTON, J. P. & NISHI, M. 1990 Vortex generator jets – means for flow separation control. *AIAA J.* **28**, 989–994.

JUNG, W. J., MANGIAVACCHI, N. & AKHAVAN, R. 1992 Suppression of turbulence in wall-bounded flows by high-frequency spanwise oscillations. *Phys. Fluids* A **4**, 1605–1607.

KIM, H. T., KLINE, S. J. & REYNOLDS, W. C. 1971 The production of turbulence near a smooth wall in a turbulent boundary layer. *J. Fluid Mech.* **50**, 133–160.

KRESOV, R. O. & PLESNIAK, M. W. 1999 Modification of near-wall structure in a three-dimensional turbulent boundary layer. In *Proc. 1st Intl Symp. on Turbulence and Shear Flow, Santa Barbara, CA, USA* (ed. S. Banerjee & J. K. Eaton), pp. 12–15. Begell House.

LAADHARI, F., SKANDAJI, L. & MOREL, R. 1994 Turbulence reduction in a boundary layer by a local spanwise oscillating surface. *Phys. Fluids* **6**, 3218–3220.

LEE, T., FISHER, M. & SCHWARZ, W. H. 1993 Investigation of the stable interaction of a passive compliant surface with a turbulent boundary layer. *J. Fluid Mech.* **257**, 373–401.

ONORATO, M., IUSO, G., DI CICCA, G. M. & SPAZZINI, P. G. 2000 Turbulence control in near wall flows. *AIAA Paper* 2000-2659.

ONORATO, JR., M. & IUSO, G. 2001 PDFs and 'plus' and 'minus' structure functions in a turbulent boundary layer. *Phys. Rev.* E **63**, 1–4, Rapid Communication.

PANTON, R. L. (Ed.) 1997 *Self-Sustaining Mechanisms of Wall Turbulence*. Advances in Fluid Mechanics, vol. 15. Southampton, UK: Computational Mechanics Publications.

PARK, J. & CHOI, H. 1999 Effects of uniform blowing and suction from a spanwise slot on a turbulent boundary layer flow. *Phys. Fluids* **11**, 3095–3105.

SAVILL, A. M. & MUMFORD, J. C. 1988 Manipulation of turbulent boundary layers by outer-layer devices: skin friction and flow visualization results. *J. Fluid Mech.* **191**, 389–417.

SCHOPPA, W. & HUSSAIN, F. 1997 Genesis and dynamics of coherent structures in near-wall turbulence: a new look. In *Self-Sustaining Mechanisms of Wall Turbulence* (ed. R. L. Panton). Advances in Fluid Mechanics, vol. 15, pp. 385–422. Southampton, UK: Computational Mechanics Publications.

SCHOPPA, W. & HUSSAIN, F. 1998 A large-scale control strategy for drag reduction in turbulent boundary layers. *Phys. Fluids* **10**, 1049–1051.

SCHOPPA, W. & HUSSAIN, F. 2000 Coherent structures dynamics in near-wall turbulence. *Fluid Dyn. Res.* **26**, 119–139.

SHAH, D. A. & ANTONIA, R. A. 1987 Scaling of wall shear stress fluctuations in a turbulent duct flow. *AIAA J.* **25**, 22–29.

SMITH, C. R. & WALKER, J. D. A. 1997 Sustaining mechanisms of turbulent boundary layers: the role of vortex developments and interactions. In *Self-Sustaining Mechanisms of Wall Turbulence* (ed. R. L. Panton). Advances in Fluid Mechanics, vol. 15, pp. 13–47. Southampton, UK: Computational Mechanics Publications.

SOLDATI, A., FULGOSI, M. & BANERJEE, S. 1999 On the use of large scale vortical streamwise structures to control turbulence in channel flow. In *Proc. 1st Intl Symp. on Turbulence and Shear Flow, Santa Barbara, CA, USA* (ed. S. Banerjee & J. K. Eaton). Begell House.

SPAZZINI, P. G., IUSO, G., ONORATO, M. & ZURLO, N. 1999 Design, test and validation of a probe for time-resolved measurement of skin friction. *Measur. Sci. Tech.* **10**, 631–639.

SUMITANI, Y. & KASAGI, N. 1995 Direct numerical simulation of turbulent transport with uniform wall injection and suction. *AIAA J.* **33**, 1220–1228.

WALEFFE, F. & KIM, J. 1997 How streamwise rolls and streaks self-sustain in a shear flow. In *Self-Sustaining Mechanisms of Wall Turbulence* (ed. R. L. Panton). Advances in Fluid Mechanics, vol. 15, pp. 309–332. Southampton, UK: Computational Mechanics Publications.

WEI, T. & WILLMARTH, W. W. 1989 Reynolds-number effects on the structure of a turbulent channel flow. *J. Fluid Mech.* **204**, 57–95.

YOSHIDA, H., KOBAYASHI, K. P., TADA, S., HIGUCHI, K., NOZAKI, T. & ECHIGO, R. 1999 Responses of low and high-speed streaks to injection or suction in a minimal flow unit. In *Proc. 1st Intl Symp. on Turbulence and Shear Flow, Santa Barbara, CA, USA* (ed. S. Banerjee & J. K. Eaton), pp. 1333–1338. Begell House.

ZHOU, J., MEINHART, C. D., BALACHANDAR, S. & ADRIAN, R. J. 1997 Formation of coherent hairpin packets in wall turbulence. In *Self-Sustaining Mechanisms of Wall Turbulence* (ed. R. L. Panton). Advances in Fluid Mechanics, vol. 15, pp. 109–134. Southampton, UK: Computational Mechanics Publications.